

UNIVERSITY OF CALGARY

Remotely Triggered Slab Avalanches

by

Benjamin Crane Johnson III

A THESIS

**SUBMITTED TO THE FACULTY OF GRADUATE STUDIES
IN PARTIAL FULFILLMENT OF THE REQUIREMENTS FOR THE
DEGREE OF MASTER OF SCIENCE**

DEPARTMENT OF CIVIL ENGINEERING

CALGARY, ALBERTA

December, 2000

© Benjamin Crane Johnson III 2000



**National Library
of Canada**

**Acquisitions and
Bibliographic Services**

**395 Wellington Street
Ottawa ON K1A 0N4
Canada**

**Bibliothèque nationale
du Canada**

**Acquisitions et
services bibliographiques**

**395, rue Wellington
Ottawa ON K1A 0N4
Canada**

Your file Votre référence

Our file Notre référence

The author has granted a non-exclusive licence allowing the National Library of Canada to reproduce, loan, distribute or sell copies of this thesis in microform, paper or electronic formats.

The author retains ownership of the copyright in this thesis. Neither the thesis nor substantial extracts from it may be printed or otherwise reproduced without the author's permission.

L'auteur a accordé une licence non exclusive permettant à la Bibliothèque nationale du Canada de reproduire, prêter, distribuer ou vendre des copies de cette thèse sous la forme de microfiche/film, de reproduction sur papier ou sur format électronique.

L'auteur conserve la propriété du droit d'auteur qui protège cette thèse. Ni la thèse ni des extraits substantiels de celle-ci ne doivent être imprimés ou autrement reproduits sans son autorisation.

0-612-64998-9

Canada

Abstract

Remotely triggered avalanches and whumpfs are commonly observed in many mountain ranges, but have received little research attention in the past. These events are generally associated with persistent weak snowpack layers.

Remotely triggered avalanches and whumpfs are contrasted to avalanches that were not remotely triggered. Significant differences were found in snowpack properties of both the weak layer and the overlying slab. Additional experimental data collected at the sites of whumpfs indicate that fracture of the weak layer is coupled to bending of the overlying slab. An experimental technique was developed to measure the propagation speed of this coupled system. The measured speed was 19.9 m/s, substantially slower than estimated values. A theory is presented that explains this propagation phenomenon. Critical to this theory is the collapse of a weak layer when fractured, and bending of the overlying slab. Experimental data are presented to support this theory.

Acknowledgements

Dr. Bruce Jamieson provided support for this thesis, both financial and through advice and supervision. This thesis would not have been possible without his commitment to avalanche research. I would also like to thank Dr. Colin Johnston for co-supervision.

For their careful field work, I would like to thank Jill Hughes, Greg Johnson, Tom Chalmers, Michelle Gagnon, Torsten Geldsetzer, Phil Hein, Alan Jones, Kalle Kronholm, Paul Langevin and Adrian Wilson,. For supplying geophysical equipment, I would like to thank Mitchem Canada, Ltd. For their support and daily advice I thank Jeff Boderchuck, Eric Dafoe, Jeff Goodrich, John Kelly, Bruce McMahon, Dave Skjönsberg, John Schliess and Steve Thomas. I would like to thank Dr. Bruce Jamieson for photos on page two and three.

Finally I would like to thank my family and friends for their encouragement throughout this project.

TABLE OF CONTENTS

| | |
|--|-----------|
| Approval Page..... | ii |
| Abstract..... | iii |
| Acknowledgements..... | iv |
| Table of Contents..... | v |
| List of Tables..... | viii |
| List of Figures..... | x |
| List of Symbols..... | xi |
| 1 INTRODUCTION..... | 1 |
| 1.1 Types of Avalanches..... | 2 |
| 1.2 Weak Snowpack Layers..... | 5 |
| 1.3 Snow Profiles..... | 7 |
| 1.4 Objectives and Outline..... | 9 |
| 2 LITERATURE REVIEW..... | 11 |
| 2.1 Introduction..... | 11 |
| 2.2 Slab Avalanche Failure..... | 11 |
| 2.3 Whumpfs..... | 15 |
| 2.4 Field Tests..... | 18 |
| 2.4.1 Cantilever Beam Test..... | 18 |
| 2.4.2 Shear Frame Test..... | 20 |
| 2.5 Fracture Propagation..... | 21 |
| 2.6 Acoustic and Seismic Sensing of Snow..... | 22 |
| 2.7 Summary..... | 23 |
| 3 EXPERIMENTAL METHODS..... | 25 |
| 3.1 Study Areas..... | 25 |
| 3.2 Cantilever Beam Test..... | 26 |
| 3.3 Shear Frame Test..... | 28 |
| 3.4 Compression Test..... | 29 |
| 3.5 Rutchblock Test..... | 30 |
| 3.6 Whumpf Investigation..... | 31 |
| 3.7 Investigation of Skier-Triggered Avalanches..... | 34 |
| 3.7.1 Slab Load..... | 34 |
| 3.8 Fracture Propagation Velocity..... | 35 |
| 4 CONTRASTING WHUMPFS AND REMOTELY TRIGGERED AVALANCHES WITH AVALANCHES NOT REMOTELY TRIGGERED..... | 38 |
| 4.1 Introduction..... | 38 |
| 4.2 Variables..... | 38 |
| 4.3 Data for Whumpfs and Remotely Triggered Avalanches..... | 39 |
| 4.4 Data for Non-remotely Triggered Avalanches..... | 41 |

| | |
|---|-----------|
| 4.5 Contrast of Remotely Triggered Avalanches to Avalanches that were not Remotely Triggered..... | 41 |
| 4.5.1 Introduction..... | 41 |
| 4.5.2 Comparison of Field Measured Variables..... | 41 |
| 4.5.3 Comparison of Stability Index..... | 44 |
| 4.5.4 Comparison of Average Slab Hardness..... | 45 |
| 4.6 Weak Layer Crystal Type for Remote and Non-Remotely Triggered Avalanches..... | 46 |
| 4.7 Discussion of Differences Between Remotely Triggered and Non-Remotely Triggered Avalanches..... | 48 |
| 5 PROPAGATION MEASUREMENTS AND CANTILEVER BEAM AT SITES OF WHUMPFs AND REMOTELY TRIGGERED AVALANCHES.... | 51 |
| 5.1 Introduction..... | 51 |
| 5.2 Propagation Distance of Weak Layers..... | 51 |
| 5.2.1 Sources of Error for Propagation Distance Measurements..... | 53 |
| 5.2.2 Fracture Propagation Stopping Condition..... | 53 |
| 5.3 Change in Thickness of the Weak Layer..... | 54 |
| 5.4 Measurement of the Propagation Speed of Fracture Through a Weak Snowpack Layer..... | 55 |
| 5.4.1 Location and Description of Experimental Setup..... | 55 |
| 5.4.2 Snow Conditions..... | 57 |
| 5.4.3 Observations and Results..... | 57 |
| 5.4.4 Discussion..... | 59 |
| 5.5 Cantilever Beam Test at Whumpf Sites..... | 61 |
| 5.5.1 Introduction..... | 61 |
| 5.5.2 Variability and Number of Tests for Required Precision..... | 61 |
| 5.5.3 Correlation Between Calculated Beam Number and Average Slab Density..... | 63 |
| 5.5.4 Qualitative Differences for Cantilever Beam Tests at Whumpfs..... | 65 |
| 5.5.5 Quantitative Differences for Cantilever Beam Tests at Whumpfs..... | 66 |
| 5.6 Conclusions..... | 68 |
| 6 THEORY FOR WEAK LAYER FAILURE ON LOW-ANGLE TERRAIN..... | 69 |
| 6.1 Introduction..... | 69 |
| 6.2 Application of Previous Avalanche Release Theories to Whumpfs..... | 70 |
| 6.3 New Theory for Avalanche Initiation on Low Angled Terrain..... | 72 |
| 6.4 Flexural Waves Through the Overlying Slab..... | 73 |
| 6.5 Fracture of the Weak Layer as Result of the Bending Slab..... | 77 |
| 6.6 Energy Considerations..... | 81 |

| | |
|--|-----------|
| 6.7 Source of Sound from a Whumpf..... | 82 |
| 6.8 Discussion..... | 83 |
| 7 CONCLUSIONS..... | 86 |
| 8 RECOMMENDATIONS FOR FURTHER RESEARCH..... | 88 |
| REFERENCES..... | 89 |
| APPENDIX A..... | 97 |

LIST OF TABLES

| No. | Title | Page |
|-----|---|------|
| 4.1 | Normality test for data collected at whumpfs and remotely triggered avalanches..... | 40 |
| 4.2 | Normality test for data collected at non-remotely triggered avalanches..... | 42 |
| 4.3 | Comparison of non normally distributed variables using the U test..... | 44 |
| 4.4 | Variables that showed significant differences..... | 49 |
| 5.1 | Thickness of weak layer before and after a whumpf..... | 55 |
| 5.2 | Distance from whumpf trigger point to each geophone, with arrival time of surface displacement..... | 58 |
| 5.3 | Measured wave propagation velocities..... | 60 |
| 5.4 | Number of cantilever beams tests required for precision..... | 63 |
| 6.1 | Weak layer fracture properties for different overlying slab ages..... | 85 |
| A.1 | Comparison of remotely triggered avalanches to avalanches not remotely triggered using the Kolmogorov-Smirnov test..... | 98 |

LIST OF FIGURES

| No. | Title | Page |
|-----|--|------|
| 1.1 | Point release avalanche..... | 2 |
| 1.2 | Slab avalanche..... | 3 |
| 1.3 | Two small remotely triggered avalanches..... | 4 |
| 1.4 | A weak snowpack layer consisting of surface hoar crystals..... | 6 |
| 1.5 | Surface hoar snow crystals (10 mm grid)..... | 7 |
| 1.6 | Faceted snow crystal..... | 7 |
| 1.7 | Inserting a fist into the snowpack to determine the layer's hand hardness..... | 8 |
| 2.1 | Schematic of a slab avalanche release..... | 12 |
| 2.2 | Diagram showing fracture in the weak layer propagating into avalanche terrain..... | 14 |
| 2.3 | Photograph of the weak layer at the site of a whumpf..... | 17 |
| 2.4 | Diagram of three point loading | 18 |
| 3.1 | Location of study sites and mountain ranges..... | 25 |
| 3.2 | Schematic of the cantilever beam test showing the beam isolated in the snow pit wall..... | 27 |
| 3.3 | Saw developed for the cantilever beam test..... | 28 |
| 3.4 | Shear frame technique..... | 28 |
| 3.5 | Compression test technique..... | 29 |
| 3.6 | Rutchblock isolated on all sides, with dimensions and loading locations..... | 30 |
| 3.7 | Picture of a perimeter crack..... | 33 |
| 3.8 | Bison geophone recorder used to measure velocity of fracture propagation in a weak snowpack layer..... | 36 |
| 4.1 | Comparison of the weak layer crystal type for remotely triggered avalanches and avalanches not remotely triggered..... | 47 |
| 5.1 | Weak layer fracture propagation distance at whumpf sites..... | 52 |
| 5.2 | Weak layer fracture propagation distance at remotely triggered avalanche sites..... | 52 |
| 5.3 | Perimeter crack of a whumpf showing surface displacement (3-4 mm) corresponding to collapse of the weak layer..... | 54 |
| 5.4 | Experimental setup to record fracture propagation velocity..... | 56 |
| 5.5 | Signal traces produced by the Bison recorder indicating the time of arrival for fracture in the weak layer. Vertical lines represent 10 ms..... | 58 |
| 5.6 | Frequency distribution for the set of 30 cantilever beam tests..... | 62 |

| | |
|--|----|
| 5.7 Cantilever beam tests for beams, 25 cm and 50 cm thick. Error bars represent one standard deviation..... | 64 |
| 5.8 Cantilever beam fracture (above) typical fracture when no weak layer is present (below) typical fracture when a weak layer is present..... | 65 |
| 5.9 Cantilever beam tests performed at sites with and without weak layer..... | 67 |
| 6.1 Model of slab avalanche failure..... | 70 |
| 6.2 Schematic of the proposed theory for whumpfs and remotely triggered avalanches..... | 73 |
| 6.3a Beam undergoing transverse motion..... | 74 |
| 6.3b Bending and shear forces acting on a beam element..... | 74 |
| 6.4 Bending of the overlying slab showing one wavelength..... | 77 |
| 6.5 One half of the bending overlying slab. It is assumed that the ends are fixed and that the length is one half of the wavelength in the slab..... | 78 |
| 6.6 Free body diagram for a beam with both ends fixed..... | 78 |
| 6.7 Schematic of the slab-weak layer interface for the cantilever beam and a bending wave in the | 79 |
| 6.8 Bending of the overlying slab resulting in fracture on the weak layer..... | 80 |
| 6.9 Plan view of fracture propagation in the weak layer coupled to the downward displacement of the overlying slab..... | 82 |

LIST OF SYMBOLS

| | |
|---------------|--|
| γ | wavenumber |
| ε | strain |
| λ | wavelength |
| π | pi |
| ρ | mass density |
| σ | normal stress |
| ω | angular frequency |
| Ψ | angle between the snow surface and horizontal |
| A | cross sectional area |
| B | beam number |
| c_0 | phase velocity |
| d | displacement of the overlying slab |
| D | amplitude of a harmonic flexural wave |
| E | Young's modulus |
| g | acceleration due to gravity |
| h | slab thickness measured perpendicular to surface |
| I | moment of inertia |
| k | coefficient to correct for non symmetrical stress in the overlying slab for the cantilever beam test |
| L | length of bending wave |

LIST OF SYMBOLS, CONTINUED

| | |
|--------|---|
| L_b | length of cantilever beam |
| m | mass per unit area |
| M | moment |
| n, N | number of data |
| p | probability associated with a statistic, significance level |
| P | precision expressed as a fraction of the mean |
| R | rank sum of data |
| s | standard deviation |
| t | time |
| T | student t |
| u | standard normal |
| U | Mann-Whitney U statistic |
| v | coefficient of variation |
| V | shear force |
| w | width of cantilever beam |
| W | Shapiro-Wilk W statistic |
| x | coordinate parallel to the snow surface |
| y | coordinate perpendicular to the snow surface |

1. Introduction

Avalanches are one threat that backcountry travelers face when they enter the mountains. They are a hazard that varies both temporally and spatial throughout a mountain range. This thesis is dedicated to investigating one particular type of avalanche that has received little attention in the past. The following excerpt gives insight to the nature of this particular avalanche problem.

“The two workers snowshoed over one avalanche deposit and heard numerous “whumpfs” as fractures spread through the weak layer. About 200 m above the highway, they discussed returning because of the avalanche danger but decided to snowshoe up one more small slope before skiing down. As they traversed a bench, they triggered an avalanche on the slope above the bench.”

Avalanche Accidents in Canada Volume 4 1984-1996

Bruce Jamieson and Torsten Geldsetzer (1996)

Many people find that it is counter-intuitive to be able to trigger a snow avalanche from the valley below a suspect slope although it is documented to occur (e.g., McClung and Shaerer, 1993). These two men were on a bench, level terrain, and remotely

triggered an avalanche above their location. The cause of avalanche release is known as the trigger.

A recent questionnaire given to avalanche professionals revealed that remotely triggered avalanches similar to the event described above accounted for forty one percent of unexpected avalanches that they recalled (Jamieson and Geldsetzer, 1999). This thesis investigates remotely triggered avalanches in order to improve our understanding and ability to forecast these events.



*Figure 1.1 Point release avalanche.
Ice Fields Parkway, Bruce Jamieson photo.*

1.1 Types of Avalanches

There are two types of avalanche release. The first is a point release avalanche (Figure 1.1) and the second is a slab avalanche (Figure 1.2). Point release avalanches are similar to the failure of a cohesionless sand slope (Perla, 1980). The failure originates in one location and as the mass descends the avalanche spreads outwards. Slab avalanches behave much differently. A cohesive slab of snow begins to slide before it breaks up. Slab avalanches are the more hazardous of the two types. Jamieson

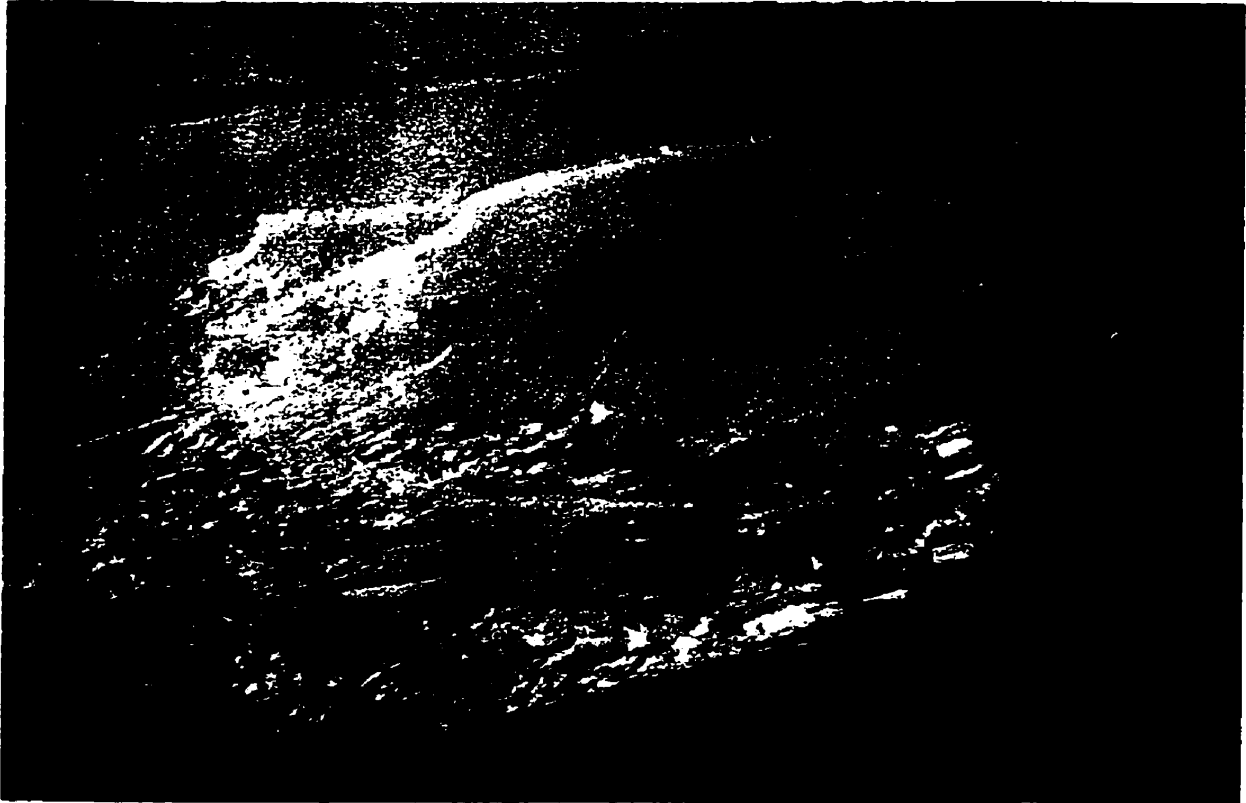


Figure 1.2 Slab avalanche. Bruce Jamieson photo.

and Johnston (1992a) report that 99 % of fatal avalanches in Canada between 1972 and 1991 were slab avalanches. For the purpose of this thesis, three types of human-triggered slab avalanche releases are identified; remotely triggered slab avalanches, slab avalanches not remotely triggered and whumpfs. Strictly speaking, a whumpf is not an avalanche but a sound indicating failure of the snowpack and is discussed in this section.

Seligman (1936 p. 334) mentions that avalanches can be triggered by a traveler at some distance from the snow slope. A remotely triggered avalanche is one where the trigger is not located in, or adjacent to the initial slab of snow that is released. A measurable distance exists between the trigger point and the site where the slab avalanche releases. Quite often, remotely triggered avalanches are triggered from below, and the location of the trigger is overrun by the slab avalanche.

Avalanches that are not remotely triggered occur much more frequently than remotely triggered avalanches. This type of slab avalanche is one where the trigger of the avalanche is directly connected to the initial slab that is released i.e. the slope on which the trigger is located avalanches.

Fractures within weak snowpack layers on horizontal terrain are widely observed by professionals who work in snow-related industries and by winter recreationists.

Typically, a person on foot, snowshoes, skis or oversnow machine initiates a fracture in a weak snowpack layer, which usually has a thickness of 10 to 100 mm. Downward displacement of the snow surface is often noticeable. This fracture propagates outwards



Figure 1.3 Two small remotely triggered avalanches. Ski poles mark the trigger location.. The weak layer fracture propagated outwards remotely triggering two unsupported rolls in the background. The slope angle varied from zero to ten degrees. Glacier National Park, British Columbia, Applied Snow and Avalanche Consortium (ASARC) photo.

from the trigger point, producing a distinctive “whumpf” sound. Although the terms *firn quake* and *settlement* have been used for the phenomenon, the onomatopoeic term *whumpf* will be used. The term *firn quake* is not well suited to seasonal snow and *settlement* is best restricted to the gradual compaction of snow layers due to gravity and granular metamorphism. In this thesis, a whumpf is defined as a fracture in a weak snow layer that propagates outwards from the trigger, but does not release an avalanche.

The failure mechanism driving weak layer fractures for whumpfs and remotely triggered avalanches is similar. Figure 1.3 provides an excellent example of these two events. The figure shows the location of a whumpf that propagated outward from the location where the whumpf was triggered. In two local spots where the slope angle was steep enough, small remotely triggered slab avalanches were initiated. This photo (Figure 1.3) clearly shows that whumpfs and remotely triggered avalanches are similar. A whumpf is a failure of the weak layer. If the overlying snow moves, it is an avalanche.

1.2 Weak Snowpack Layers

One of the conditions that must exist for a slab avalanche to occur is a weak snowpack layer or interface within the snowpack (e.g. McClung, 1987). A snowpack layer is considered weak if it is weaker than adjacent snowpack layers (Figure 1.4). There are two types of weak snowpack layers (Jamieson, 1995), non-persistent weak layers and persistent weak layers. Non-persistent weak layers usually consist of newly fallen snow and generally stabilize within a few days. The second type, persistent weak



Figure 1.4 A weak snowpack layer consisting of surface hoar crystals. Vowell Creek, Purcell Mountains, ASARC photo.

snowpack layers, can persist for weeks and even months in the snowpack, providing a potential failure plane for avalanches and whumpfs. Persistent weak layers form within the snowpack and can consist of the three following snow crystals: surface hoar, facets and depth hoar. Whumpfs and remotely triggered avalanches tend to occur only when a persistent weak snowpack layer is present (Johnson et al., 2000).

Surface hoar crystals form during clear cold nights. The snow's surface cools rapidly as a result of long wave radiation emission. Surface cooling creates a strong temperature gradient near the surface of the snow. Moisture in the air is deposited on the snow surface in crystal form (Figure 1.5). Surface hoar crystals can range in size from a few millimeters to several centimeters. When buried by subsequent snowfalls,

such layers form persistent weak layers in the snowpack.

Faceted crystals and depth hoar form due to a temperature gradient within the snowpack that drives kinetic growth of existing snow crystals

(Figure 1.6). The temperature gradient drives the transfer of water vapor from

one snow crystal to another snow crystal (de Quervain, 1963). Larger grains grow in the snowpack at the expense of smaller crystals. At an

intermediate stage, when flat faces exist on the snow crystal, the crystal is

considered a faceted crystal (Colbeck et al., 1990). During more advanced stages of faceted crystal growth striations form on the larger crystals. Crystals with striations are no longer considered facets, they are classified as depth hoar crystals. These can continue to metamorphose into cup and column-shaped crystals.

1.3 Snow Profiles

The snow profile is widely used by avalanche professionals to gain information about the snow pack. It is a systematic observation of snowpack layers made in a pit

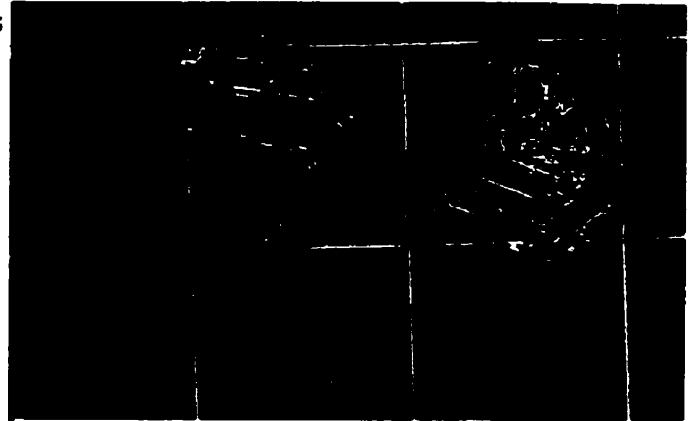


Figure 1.5 Surface hoar snow crystals. (10 mm grid) ASARC photo.

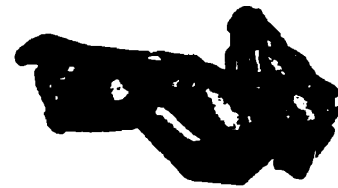


Figure 1.6 Faceted snow crystal. ASARC photo.



Figure 1.7 Inserting a fist into the snowpack to determine the layer's hand hardness . ASARC photo.

dug where the snowpack is undisturbed (CAA, 1995). The main objective of a snow profile is to examine the layering of the snowpack and identify weak snow layers. Thickness, crystal type and crystal size are recorded for each snow layer. A hardness measurement is also taken for each snow layer. “Hand hardness” is a simple and effective field measure of a snow layer’s hardness. Hardness is determined by inserting objects of different size into the snowpack (Figure 1.7) . The objects from largest to smallest are: fist, four fingers, one finger, pencil and knife. The snow layer is assigned a hardness level corresponding to the object which takes 10 to 15 N of force to insert.

In addition to information gathered about layering within the snowpack, a temperature profile is taken through the snowpack and the height of the snowpack and the slope angle are measured. The snow temperatures are taken immediately upon excavation of the snow pit with digital thermometers placed 25 cm into the snow wall. Often a stability test is performed in conjunction with the snow profile. Two examples

of stability tests are the compression test and the rutchblock test. These are described in Chapter 3.

1.4 Objectives and Outline

The objectives of this thesis are:

- to collect data at the sites of whumpfs and remotely triggered avalanches to understand remotely triggered avalanches better. Remotely triggered avalanches are a problem that has been identified for years, but has yet to be the focus of a research project.
- to compare whumpfs and remotely triggered avalanches to avalanches not remotely triggered using easily measured snow pack variables.
- to develop a theory for whumpfs and remotely triggered avalanches that explains weak layer fracture propagation on low angle terrain.

A majority of the work performed in this thesis was collecting data so that whumpfs and remotely triggered avalanches could better be described and also compared to avalanches that were not remotely triggered.

Chapter 2 reviews relevant literature on whumpfs and remotely triggered avalanches. Literature regarding the cantilever beam test, shear frame test, fracture propagation and acoustic and seismic sensing of snow are also reviewed. Field methods are introduced in Chapter 3. Whumpfs and remotely triggered avalanches are contrasted in Chapter 4 to avalanches that are not remotely triggered, using easily measured snowpack variables and several calculated indices in Chapter 4. Chapter 5 presents additional data that were

collected at investigated whumpf sites: including the measured collapse of the weak layer, the speed of weak layer fracture propagation and cantilever beam test results. A new theory for weak layer fracture propagation on low angled terrain is introduced in Chapter 6. Chapters 7 and 8 include conclusions and ideas for future research respectively.

2 Literature Review

2.1 Introduction

This thesis investigates the occurrence of whumpfs and remotely triggered avalanches. An overview of the literature relating to slab avalanche initiation is presented in Section 2.1. Literature on whumpfs is reviewed in Section 2.2. During the field investigation, the properties of both the weak layer and overlying slab were measured using the shear frame test and cantilever beam test respectively. Research relevant to these two field tests is presented in Section 2.3. In addition to these field tests, the propagation speed of fracture through a weak snowpack layer was measured using seismic recording equipment. Previous research on fracture propagation through snow is reviewed in Section 2.4, while snowpack research involving seismic recording equipment section is discussed in Section 2.5.

2.2 Slab Avalanche Failure

When a slab avalanche releases, failures occur on five surfaces: one in tension at the top of the slab, two lateral shear breaks on the sides of the slab, one compressive failure at the toe of the slab and a failure between the slab and the supporting superstratum (Figure 2.1). Bucher (1948) and Roch (1956) proposed that one of these fractures could be considered the primary rupture with the other four following and

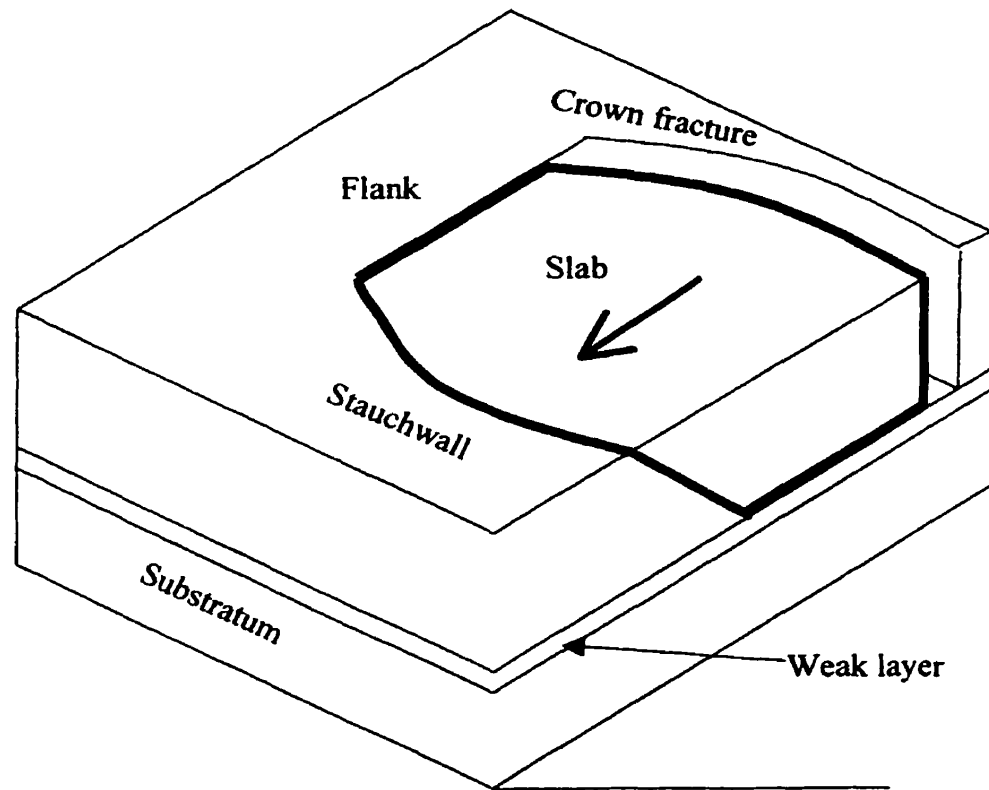


Figure 2.1 Schematic of a slab avalanche release.

called secondary failures. In addition, Roch (1956) reports that not only could there be a shear failure between the overlying slab and the supporting substratum, but there could also be a collapse of the weak layer, which is accompanied by “a resonant noise well known to skiers.” He emphasized that the shear strength of weak layers in relation to the stress imposed by the overlying slab was the most important relationship determining the stability of a slope.

Prior to 1970, there was no consensus on which failure occurred first when an avalanche was initiated. Haefeli (1963, 1967) believed that tensile fracture at the crown was the initial and most important failure. Bradley and Bowles (1967) followed Roch’s work and focused on compressive failure within a weak layer beneath the slab. Their

work considered thick layers of depth hoar, while Roch (1956) considered thinner weak layers. Bradley and Bowles (1967) used limited field data to correlate a relationship between resistance-to-vertical-penetration and vertical stress due to slab weight with avalanching initiated by the collapsing of thick depth hoar layers. Sommerfeld (1969) argued that the initial fracture was a tensile one that started at a flaw in the top of the snowpack. This flaw could be either natural or caused by a skier putting tracks across a snow slope. In his view, the tensile fracture starts at the surface and proceeds downward until a layer of low shear strength snow is encountered; the fracture then propagates along this layer as the upper layers contract elastically. For these brittle fractures to occur either the applied load increases rapidly or high strain rates are present. Sommerfeld addresses avalanches which “settle in place”, stating that the vertical cracks dissipate the tensile stress in the snowpack leaving no stress to propagate shear fractures.

In 1970, Perla and LaChapelle made a compelling argument that the first failure in a slab occurred due to a loss of shear support. They argued, however, that the first *fracture* is a tensile crown fracture. In their theory, the basal failure is ductile leading to increased stress in the crown region followed by a brittle crown fracture that extends into the basal weak layer.

McClung’s (1981, 1987) work focused on ductile shear failure of the weak layer followed by shear fracture and propagation through the weak layer at the base of the slab and consequent tensile crown fracture. Other researchers have also assumed that shear fracture occurs first (Gubler and Bader, 1989; Bader and Salm, 1990).

A complete review of dry snow avalanche release was presented by Schweizer in

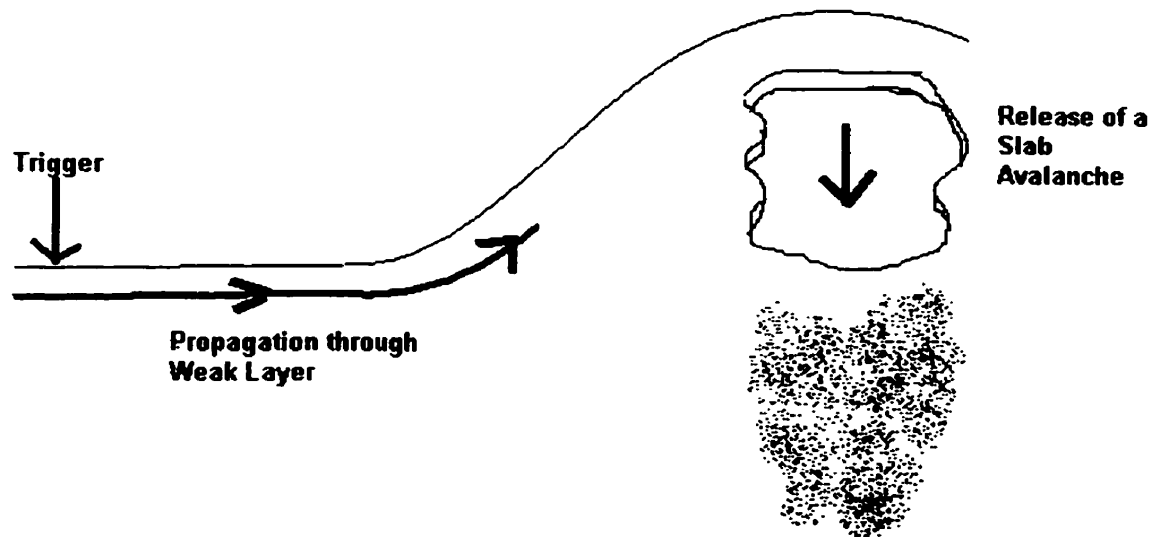


Figure 2.2 Diagram showing fracture in the weak layer propagating into avalanche terrain.

1999. He concluded that while the initial failure in the weak layer was most commonly accepted as a shear failure, it was quite plausible that the initial failure in the weak layer could be a compressive failure. All of the models he reviewed were of two-dimensional inclined snowpack with an assumed prior weakness existing in the otherwise homogenous weak layer.

To date no experimental or theoretical research has been presented that would explain failure in a weak layer propagating through *horizontal* terrain. The mechanisms presented above all require inclination of the snowpack. Whumpfs can, and often do occur in horizontal areas. These fractures can propagate through the weak layer onto slopes steep enough to release a slab avalanche (Figure 2.2). Jamieson and Geldsetzer (1996) report numerous incidents where avalanches on steeper slopes were initiated by

fracture propagation from adjacent slopes with only a slight incline. Lackinger (1989) provides an explanation for whumpfs, with no supporting details. He reports that the collapse of a weaker layer could subject the slab to bending forces, with the area of bending widening along with the lateral propagation of the collapse to the point where the slope becomes steep enough to release a slab avalanche. Fracture of the slab on a slope becomes unavoidable.

2.3 Whumpfs

Numerous informative avalanche books refer to whumpfs as predictors of instability (McClung and Schaerer, 1993; Armstrong and Williams, 1992; Fredston and Fessler, 1994). Other researchers have mentioned them briefly in dealing with release mechanisms (Bader et. al, 1954; Roch, 1956; Lackinger, 1989). Seligman (1936) discusses the release of avalanches due to the passage of skiers at some distance below a threatening slope. He offers no explanation, but does state that these distant releases of avalanches do occur. He presents three cases, and concludes that further study is needed. Truman (1973) gives the first detailed account of human triggered whumpfs. He reports being able to see the wave front traveling across the snow surface in conjunction with a continuous “swishing” sound that could be heard traveling away from the start of the whumph and decreasing in intensity. Observations made at the location where propagation stopped revealed a discontinuity in the snow surface with the disturbed snow 1 to 2 cm lower than the undisturbed snow just ahead of the discontinuity. An estimate for the speed of the waves was 6 m/sec. The snow depth

was estimated at approximately 30 cm with daytime temperatures above freezing. Bohren and Beschta (1974) suspect that Truman was observing a collapse of depth hoar. They note that there does appear to be wave traveling in the snow, but the slow speeds rule out compression or shear waves. They also noted witnessing these collapses accompanied by an audible “whomphing.” Around the periphery of these areas, an irregular crack was observed at the surface.

Benson (1960) reports that while traversing Greenland, spectacular collapses of soft layers were observed when walking or digging pits in undisturbed areas. In one case a barrel dropped from an airplane penetrated the snow surface initiating one of these collapses. The collapse of a weak layer started at the point of impact and spread, accompanied by a sound. Georgi (1933) reports feeling several earthquake type events in Greenland. He reports, “on 19 February 1931, at 6:55 a.m. a noise approached rapidly; then followed a large crash; and then the noise ran away.” The snow layers at a depth of between 2 and 2.5 meters appeared to have collapsed approximately 2 centimeters.

DenHartog (1982) reports similar events in Antarctica. A 10 lb charge was set off in a 10-m hole. A vehicle located at the shot point dropped noticeably. Another person and vehicle were five miles away; they received a large ice wave shortly after the explosion. The sound waves arrived only slightly before the snow wave, indicating speeds much greater than reported by Truman (1973). Jamieson (1998) includes a photo (Figure 2.3) of the basal fracture meeting the perimeter fracture of a whumpf. The downward displacement of the area that has fractured is obvious in the photo.

During the spring of 1999, the author was ski-touring in the Chugach range of



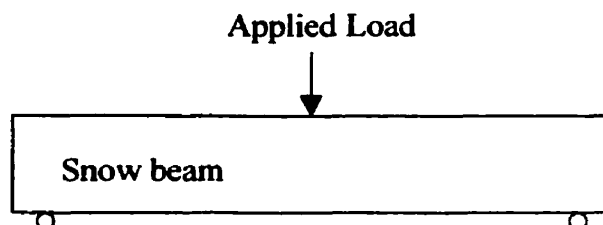
Figure 2.3 Photograph of the weak layer at the site of a whumpf. The fracture propagated from approximately 8 meters to the left. The vertical crack extends to the surface. Vowell Creek, Purcell Mountains, ASARC photo.

Alaska and witnessed several whumpfs. Similar to Truman (1973) a wave was observed to move across the surface of the snow accompanied by a sound. The snow-pack was wet.

To date there have been no studies that have focused on fracture propagation through weak layers on horizontal terrain. This thesis will focus directly on this process.

2.4 Field Tests

2.4.1 Cantilever Beam Test



One of the first beam tests on snow was performed in 1969 by Stearns using a three point loading

Figure 2.4 Diagram of three point loading (Stearns, 1969).

device (Figure 2.4). The beam was supported at each end and loaded at its midpoint. Approximately 120 samples were loaded to failure, each in less than ten seconds. The only measurement taken was the load at failure. Stearns concluded that there appeared to be a relationship between density and flexural strength for snow. He also noted that at lower densities stratification and crust layers could significantly affect the properties of the beams. His tests covered the snow density range from 400 to over 600 kg/m³, densities higher than those encountered in the upper layers of alpine snowpacks.

The first use of the *cantilever* beam test on snow was by Perla in 1969. He performed approximately 250 tests and primarily used the test to determine the tensile strength of the snow. He tested layers that were 5 cm thick and essentially homogeneous with densities ranging from 50 to 300 kg/m³. The sides of the beam were isolated and then a pan was used to remove snow from under the beam. The amount of snow removed (length of undercut) necessary to cause failure was measured. The test was carried out quickly to avoid any effects of strain softening. A beam number (B) was calculated by the following formula:

$$B = \frac{3g\rho L_b^2}{h} \quad (2.1)$$

Where L_b is the length of beam, ρ is the density and h is the thickness. B is usually related to the stress in the top fibre by

$$\sigma = kB \quad (2.2)$$

where k makes adjustments for non-symmetric stress distributions. Perla concluded that shear failure could also play a role in the failure of cantilever beams, and that more work was needed to determine if the variation of the values measured were real variations of the properties of the snow, or peculiarities of the cantilever beam test. The test, however, could prove useful in understanding the properties of the overlying slab (Perla, 1969). The method used by Perla could not be used to test the entire slab as one unit.

Mears (1998) also used the cantilever beam test to measure properties of overlying slabs. He performed 80 tests on newly fallen snow with the thickness of the beams ranging from 10 cm to 16 cm thick. Mears used the same formula as Perla to estimate the maximum tensile stress at failure. His tests were performed in less than 30 seconds, which he concluded to be sufficiently fast to place the failures in the brittle range. Mears concluded that new snow layers rapidly gained strength within 2 to 4 days after snowfall, and that avalanche activity stopped as the upper layer increased in strength by a factor of two.

Sterbenz (1998) conducted another more field-oriented test. The test required no specialized tools or recording equipment. He developed a cantilever test method that gave a numerical score based on the ability of the beam to withstand different loading conditions. The steps ranged from simply isolating a cantilever beam of snow to adding additional weight to the beam until failure. The scoring system was modeled after the

widely used Rutchblock test, with values ranging from one to seven. The results showed little correlation with avalanche activity, but did correlate with avalanche size.

The cantilever beam test has been used extensively in ice mechanics. J. Shwarz et al. (1981) report that the theory needed to determine the true flexural strength from the cantilever beam test is a complex problem due to ice being an inhomogeneous, anisotropic and elasto-viscoplastic material. However the test still provides an index value for flexural strength that can be measured in situ. Similarly, snow is an inhomogeneous, anisotropic and elasto-viscoplastic material.

2.4.2 Shear Frame Test

Shear frames have become the method of choice to measure the shear strength of weak layers in the snowpack quantitatively. Roch (1956) first used the shear frame to measure the strength of weak layers. Perla (1977) used shear frames of different sizes to determine the shear strength of weak layers. He found that larger frames give lower mean strength values. Stethem and Tweedy (1981), Sommerfeld (1980), Föhn (1987) and Jamieson (1995) found similar results.

Sommerfeld (1980) proposed that Daniels (1945) thread bundle statistics could explain the size effect in the shear frame tests. Föhn (1987) then used Daniels' strength theory data compiled from previous research (Perla, 1977; Sommerfeld, 1980) to obtain a curve of correction factors. He found that for large frames the strength values asymptotically approached an arbitrary value called Daniels strength. A multiplier can be applied to strength values measured by different frame sizes to convert to the Daniels

strength.

Jamieson (1995) did extensive testing on the shear frame test. Size effects, variability between different operators, frame design, effect of normal load and frame placement techniques with respect to the weak layer were investigated to determine their effect on the measured strength values. Results from Jamieson (1995) and Jamieson and Johnston (in press) will be used in this study to utilize best the shear frame for strength measurements.

2.5 Fracture Propagation

Very little has been written about fracture propagation through snow. Gubler (1977) used acoustic and seismic sensors to monitor fractures in alpine snowpacks. He reported through experimentation that brittle fractures propagate at roughly half of the shear-wave velocity in the material. Fractures in other materials travel at approximately one third of the propagation velocities of compressional stress waves through the material (Kolsky and Rader, 1968). Kirchner et al. (2000) measured the fracture toughness of snow in tension and reported that snow is one of the most brittle materials known to man.

Bader and Salm (1990) give a numerical model that explains the propagation of shear fracture through a weak layer in the snowpack. They conclude that once brittle fracture occurs, the speed of fracture is in the order of 10^2 - 10^3 m s⁻¹, and that the extent of fracturing is controlled entirely by the tensile strength of the overlying snow layers. Jamieson and Johnston (1992b) present a model that determines the extent of fracture

propagation through weak layers. The model is based on the shear strength of weak layers, the thickness of the overlying slab and tensile strength of the overlying slab. Limited field data are presented to support the model. Propagation speed is not discussed, nor is propagation through horizontal terrain.

2.6 Acoustic and Seismic Sensing of Snow

Acoustics and seismic sensing has been used for several different applications in snow sensing. St. Lawrence and Bradley (1977) used geophones, with a natural frequency of 4.5 Hz, mounted in bedrock or attached to cement anchors in avalanche start zones and slide paths. They recorded data in two frequency bands from 30 kHz to 200 kHz and 4 Hz to 100 Hz. Emissions from the two different frequencies are significant in terms of the mechanical processes taking place in the snow cover. Emissions at the higher ultrasonic range indicate changes taking place at the granular level in the snowpack. This type of emission generally signifies a change in the state of the snowpack but is not necessarily associated with failure of a snow slope. The emissions from the lower seismic frequencies are generally indicative of a major displacement of the snowpack. These lower frequency emissions might be either catastrophic fracture of the pack that results in an avalanche or internal fracture of the snow.

Gubler (1977) used a non-resonant high-sensitivity acceleration transducer to measure similar signals recorded by St. Lawrence and Bradley (1977). Gubler's sensors were matched to the same density of weakly settled snow and placed 0.3 – 1 m below

the surface of the snow. Sommerfeld and Gubler (1983) report that the best sensor available to detect acoustic and seismic emissions is a foam-mounted geophone placed in the snowpack. The foam allows the sensor to be matched in density to the snow where it will be placed.

To date most studies using acoustics and seismic sensors has focused on using the frequency of peak emissions as an indicator of instability in the snowpack (Gubler, 1977; Sommerfeld, 1977; Leaird and Plehn, 1984) with a positive correlation being found. Sommerfeld (1982) points out that experimental technique is important when using acoustic sensors in snow, which might explain why St. Lawrence and Bradley (1977) actually reported a negative correlation between emissions and avalanche activity.

Other research has focused on using seismic recording equipment to detect occurrence of avalanches (Schaerer and Salaway, 1980; Leprettre et al., 1996). In the study described here, geophones were used to measure the fracture propagation speed in weak layers.

2.7 Summary

A review of all literature relevant to whumpfs and remotely triggered avalanches reveals no field studies that have focused on these two events. Only once in the literature is a mechanism stated that could explain how these fractures propagate through horizontal terrain but there were no supporting theory or field data. A review of the cantilever beam test shows that it has been used several times to measure the flexural

strength of snow, but that the method could still use improvement in order to measure slabs overlying weak layers as one unit. A review of the shear frame shows that it is an effective method to test the shear strength of weak snow layers. A review of fracture in snow reveals very little research in this area, with even less specifically aimed at fracture propagation through weak snowpack layers.

3 EXPERIMENTAL METHODS

3.1 Study Areas

Research for this thesis was carried out in conjunction with several other projects concurrently by the Applied Snow and Avalanche Research Group at the University of Calgary. During the winters of 1998-99 and 1999-00 researchers (graduate students and seasonal research

technicians) were based at Mike Wiegele Helicopter Skiing in Blue River, B.C. and at Rogers Pass, Glacier National Park, B.C. During the winter of 1999-00 additional experimental work was also performed at Bow Summit, Banff National Park, Alberta.

During the winters of 1997-98 and 1996-97 researchers

were based at Mike Wiegele Helicopter Skiing and at

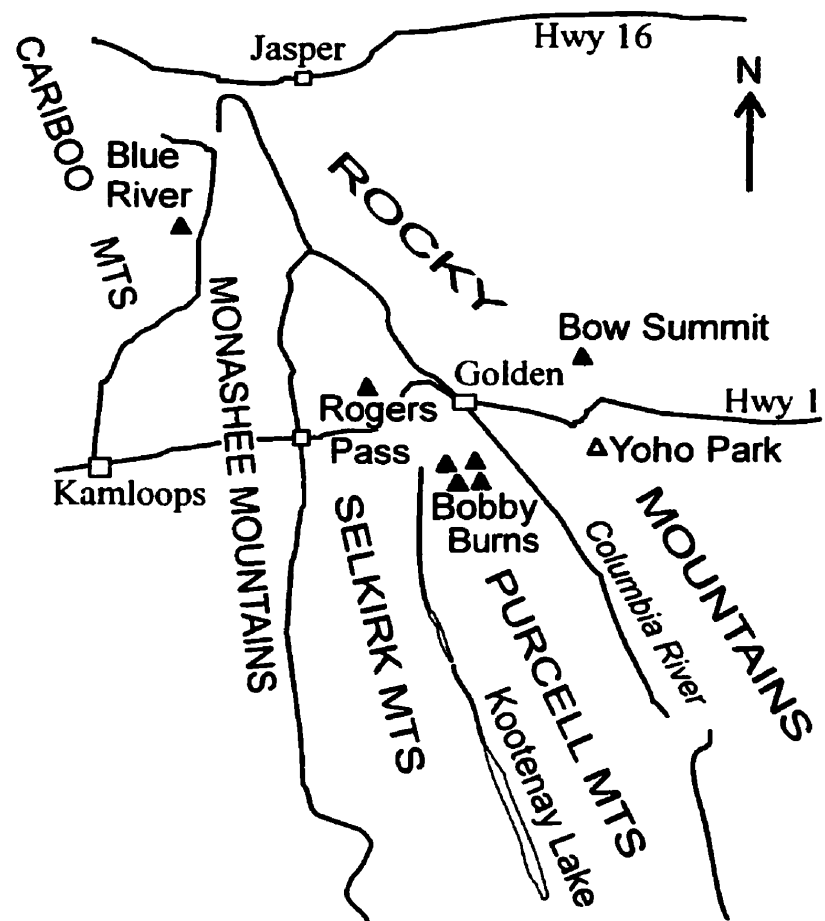


Figure 3.1 Map of study sites and mountain ranges.

Canadian Mountain Holidays Bobby Burns Lodge (Figure 3.1). Three of these sites are located in the Columbia Mountains while the fourth, Bow Summit, is located in the Rocky Mountains. Snowpack in the Columbia Mountains at tree line usually exceeds two meters in thickness during mid winter. This deep snowpack, along with relatively mild air temperatures keep temperature gradients relatively low. Weak layers composed of depth hoar are rare. Persistent weak layers in the Columbia Mountains usually consist of surface hoar or faceted crystals. The proximity of the Glacier National Park avalanche research station to the Rocky Mountains also allowed additional data to be collected in the Rocky Mountains when conditions were appropriate. The snowpack in the Rocky Mountains averages 1 – 1.5 m at tree line during mid winter. Colder temperatures and thinner snowpack contribute to temperature gradients sufficient to produce thick weak layers of depth hoar.

3.2 Cantilever Beam Test

The cantilever beam test was used because it requires equipment that can easily be carried into the field, and the test is an effective way to measure the flexural strength of snow (Perla, 1969). Disadvantages of the test are, undercut speed cannot be precisely controlled, and the test is limited to slabs less than 100 cm thick. The present study used a method that was similar to the method used by Perla (1969) and Mears (1998). The first step involves isolating a beam in the wall of a snow pit (Figure 3.2). The width is 30 cm and the length is initially 130 cm. The sides are excavated by first making two

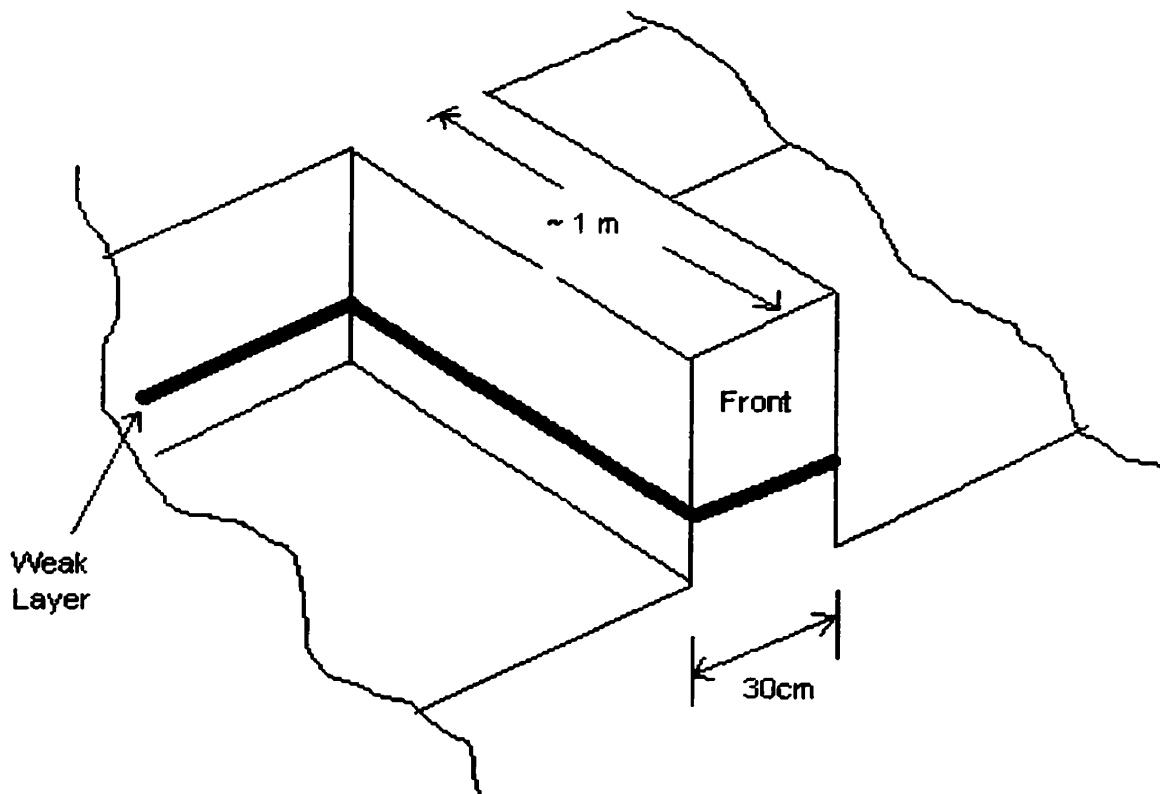


Figure 3.2 Schematic of the cantilever beam test showing the beam extending from the snow pit wall. The weak layer is undercut from the front to back using a saw developed for this test.

vertical cuts with a 130 cm collapsible saw and then shoveling around the beam without damaging the sides of the beam. The weak layer is identified and is the plane for undercutting the beam. The cantilever beam test was also performed at arbitrary depths of 25 cm and 50 cm, to test for repeatability. The beam is then undercut (using a saw developed for this study Figure 3.3) in a rapid manner, taking less than five seconds to fracture. The saw allows the cut to proceed quickly and at a constant pace. The saw cuts through the weak layer so that the overlying slab is cantilevered. The slot cut by the saw is 2 cm wide, effectively taking away support from the beam. When the beam fails, cutting stops and the saw is left in place. The length of the undercut and the depth of the

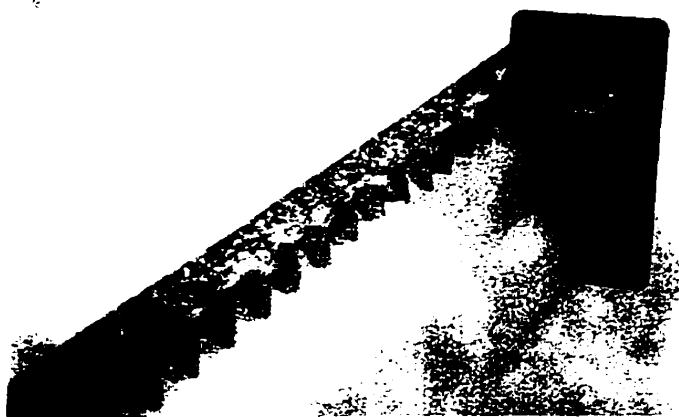


Figure 3.3 Saw developed for the cantilever beam test. It creates a two-centimeter wide slot, taking away support and cantilevering the beam. ASARC photo.

fracture from the front of the beam are measured. A sketch is drawn to record the fracture shape. The test takes approximately the same time to perform as the widely used compression test. More time goes into preparation of the beam, but the test

itself is performed in less than one minute by determining the mean length of the undercut from three repeated tests..

3.3 Shear Frame Test

The shear frame test is also easily performed in the field and measures the shear strength of weak layers in the snowpack. Jamieson (1995) developed the technique used in the current study. The weak layer is identified by visual inspection or by utilizing a field test such as a shovel test,



Figure 3.4 Shear frame technique. ASARC photo.

compression test, rutchblock test or other similar snow stability or strength test. Once the weak layer is identified, snow is removed from above the layer leaving approximately 40-45 mm of undisturbed snow. The shear frame is gently inserted into the overlying snow to within 2-5 mm of the weak layer. After placement, a thin blade is passed around the frame to ensure that the block of snow is only restrained from below the frame. The force gage is attached to a cord connected to the shear frame and pulled smoothly and quickly (Figure 3.4). Shapes of fracture and force required are recorded. Shear strength is determined by dividing the maximum load on the force gauge by the area of the frame. Seven shear frame tests are performed at field locations. With a 90% confidence, the mean shear strength can be determined with a precision of 15% from seven repeated tests (Jamieson 1995; Jamieson and Johnston, in press).

3.4 Compression Test

A column of snow 30 cm by 30 cm is isolated in the snowpit. The column extends down below the weak layer of interest (Figure 3.5). A shovel is then placed squarely on the top surface of the column. The first loading



*Figure 3.5 Compression test technique.
ASARC photo.*

sequence is to tap the shovel blade ten times with the fingertips, only moving the hand from the wrist. The second step is to tap the shovel blade ten times with the fingertips, but this time moving the arm from the elbow. The last step is to tap the shovel ten times with a closed fist, this time moving the arm from the shoulder. The taps within each step are all equal. The impact increases from the first step through the third step. When the weak layer fails, a score is given to the failure based on the number of taps preceding the failure. This score ranges from one to thirty (CAA, 1995).

3.5 Rutchblock Test

In a snow pit that is at least as deep as any potential weak layers, a large column (2 m in width and 1.5 m along the slope) is isolated in the front wall (Figure 3.6). The sides can either be shoveled out, or can be cut using a large (130 cm) snow saw. This saw can then be used to cut the upper wall. Alternatively, the column can be isolated by using the tail of a ski, or by cutting with a knotted cord stretched around probes or a ski

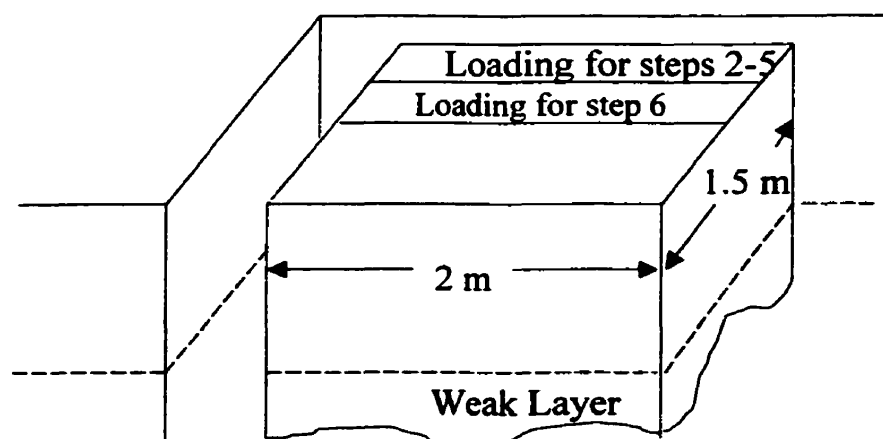


Figure 3.6 Rutchblock isolated on all sides, with dimension and loading locations.

pole at each back corner. If one of the latter methods is used the block should be 2.1 m wide in the front and 1.9 m wide in the back. This flaring reduces the potential for friction between the block and snowpack. The rutchblock is then loaded using the following sequence (Föhn 1987):

1. An undisturbed column of snow is isolated by shoveling or cutting as described above.
2. The skier approaches the block from above and gently steps down onto the upper part of the block.
3. Without lifting the heels, the skier drops from a straight leg to a bent knee position, pushing downwards.
4. The skier jumps upwards, clear of the snow surface, and lands in the same spot.
5. The skier jumps again and lands on the same spot.
6. For hard or deep slabs, the skier removes skis and jumps on the same spot. For softer slabs where jumping without skis might penetrate through the slab, the skis are kept on, the skier steps down 0.35 m – almost to mid block- and pushes downwards once then jumps at least three times.

A score is given to the test based on which loading step caused the weak layer to shear cleanly. If the layer does not fail in shear through the six loading steps then it is given the score of 7, indicating no failure (CAA, 1995).

3.6 Whumpf Investigation

Whumpfs occur only under certain conditions. During each winter, whumpfung

can be expected to occur on a widespread basis several times. Whumpfs generally occur in cycles lasting several days when the snowpack conditions are conducive to whumpfung. Technicians at both field stations monitored snowpack conditions closely, communicating with park staff and ski guides about local conditions throughout the Columbia and Rocky Mountains. It is expected that each mountain range would typically have between five and ten days per season when the snowpack was ripe for triggering whumpfs. During these days, researchers investigated whumpfs and remotely triggered avalanches.

When conditions were favourable for whumpfung, researchers traveled either by skis or helicopter to sites where whumpfs had occurred or where the technicians felt that there would be a high likelihood of initiating a whumpf. When a whumpf occurs the fracture of the weak layer and movement of the overlying slab causes vegetation protruding through the surface to exhibit visible movement. After a whumpf, the weak layer has fractured within an area often 10 m^2 to over 1000 m^2 . Determining the extent of fracture propagation (discerning between the fractured and unfractured areas) can be difficult and is not always possible. Two methods were used to determine the extent of propagation. If the whumpf was observed it may be possible to estimate the extent by the motion of vegetation protruding through the surface of the snow. After the whumpf, inspection of the snow surface may reveal perimeter cracks on the surface of the snow (Figure 3.7). At sites where the weak layer has fractured, layering and densities of the overlying slab were recorded, snowpack temperatures taken, thickness of the weak layer measured, three cantilever beam tests performed, sketches drawn of the fractured area, and the distance from the trigger to the furthest point of propagation measured. At sites



Figure 3.7 Picture of a perimeter crack. The weak layer down and to the right of the crack has fractured. This perimeter crack indicates the extent of fracture propagation in the weak layer. Bow Summit, Banff National Park, ASARC photo.

where the weak layer is unfractured similar information was recorded, along with two additional procedures. Seven shear frame tests and three compression tests were performed on the combined slab and weak layer. The change in thickness of the weak layer was also measured at sites where the extent of fracture propagation could be determined. This was done by taking several thickness measurements at an area where the weak layer had fractured and taking several thickness measurements in an area where the weak layer had not fractured. This weak layer measurement is performed to determine an average vertical displacement of the overlying slab.

3.7 Investigation of Skier-Triggered Avalanches

In addition to investigating whumpfs and remotely triggered avalanches, this study also used data from avalanches that were skier-triggered, i.e. where the skier initiated the avalanche from within the start zone. These events will subsequently be referred to as avalanches not remotely triggered. These avalanches were reported to the research staff by a guide or park service employee and investigated within one to two days after the event occurred. Occasionally the research staff was able to trigger small controlled avalanches of this type and immediately investigate the avalanche.

At the site of a skier-triggered avalanche, the following information was gathered: layering of the snowpack, snowpack temperatures, densities of the layers above the weak layer, crystal type and thickness of the weak layer. In addition, at these sites seven shear frame tests were performed on the weak layer, and three compression tests on the combined slab and weak layer, and one to two rutchblock tests were performed.

3.7.1 Slab Load

The slab load, is the weight of the slab per unit horizontal area. At avalanche and whumpf sites, slab load was determined using two methods. The first method can only be performed after all the snowpack layers in the overlying slab have been identified. A cylinder (volume 100 cm^3) is used to sample all layers greater than 4 cm in thickness. The cylinder is 93 mm long and 37 mm in diameter. If the layer was

thicker than 10 cm the sample was taken vertically, thinner layers required horizontal sampling. The samples were removed from the snowpit wall and weighed using a portable digital scale. For layers that were too thin to sample a method utilizing crystal type and hardness (Geldsetzer and Jamieson, 2000) was used to estimate the density of the layer. The slab load was then calculated by using the weighted average of each individual layer.

The second method used to measure the slab load was the “core load” method. This method uses a much larger sampling tube with cross sectional area of 0.0028 m^2 . The tube is inserted vertically into the slab. Samples are removed and placed in a nylon bag. If the slab thickness is greater than the length of the sampling tube, repeated samples must taken through the entire thickness of the slab. The tube is removed from the pit wall emptied and then reinserted into the same column continuing downward. Each complete sample of the slab would be considered one core. The nylon bag containing the samples is weighed using a force gauge. Repetitions are repeated until the bag weighs at least ten percent of the pull-gauge’s maximum measurable load. This is to ensure accurate readings. The measured weight is divided by the number of cores and the area of the tube to obtain the weight per unit area.

3.8 Fracture Propagation Velocity

To measure the speed of fracture in a weak snowpack layer, a method was developed that uses geophones and a portable seismic recorder (Figure 3.8). The idea is to place the geophones on the surface and detect the downward displacement of the slab

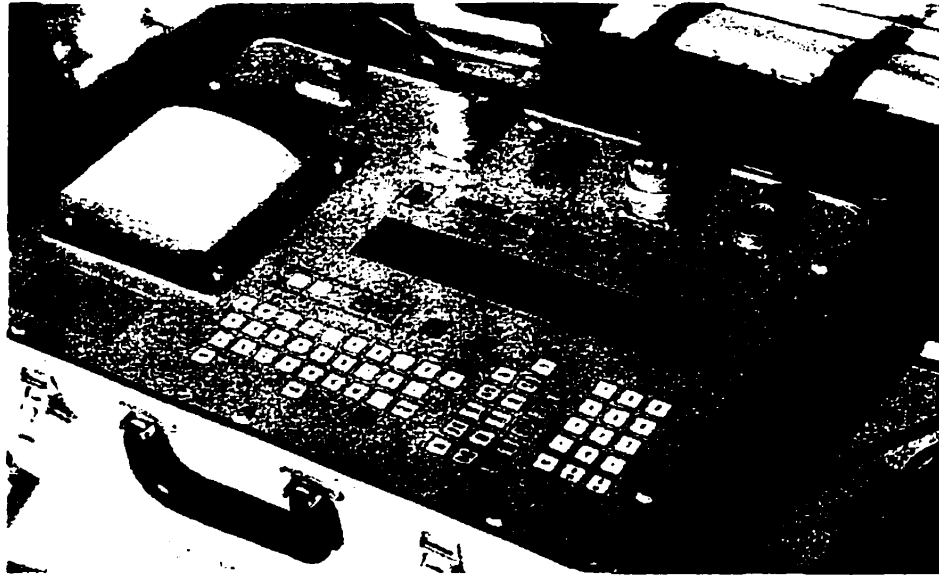


Figure 3.8 Bison geophone recorder used to measure velocity of fracture propagation in a weak snowpack layer. ASARC photo.

caused by the fracture in the weak layer. Once the geophones are in place and the recorder is running, a person on foot attempts to trigger the whumpf by walking with snowshoes on the slab. Each geophone measures the exact time that the snow surface is displaced downwards. This information, combined with the distance from each geophone to the trigger point is used to calculate the velocity. The difficulty with this experiment was that the geophones had to be placed before the whumpf occurred, requiring a strategy, careful preparation and persistence. Only one attempt over four days was successful

The geophones used were *Geospace 20* geophones. The recording equipment was a Bison digital geophone recorder (Figure 3.8), capable of sampling at 2000 Hz using six geophones for a total sample time of 10 seconds.

The first step to perform this experiment involved locating an undisturbed open area that could be approached without fracturing the weak layer. Approach paths

included, treed areas, areas already disturbed, existing trails and rocky outcrops.

Researchers often traveled in the deep snow without skis or snowshoes when approaching undisturbed sites. This allowed for foot penetration through the weak layer reducing the possibility of inadvertently triggering a whumpf before the equipment was in place. In order to place the geophones in the clearing, a rope was stretched across the open area by accessing opposite sides without whumpfing the area. This rope was then used to pull the geophones into position. Once in place the recording system was turned on. The next step was to trigger a whumpf. This was normally achieved by walking in one area, near one end of the geophone string, with either skis or snowshoes. After the whumpf was triggered, measurements were taken which give the location of the geophones relative to each other and the trigger point. The whumpf was then investigated as detailed in Section 3.2.

The velocity of the crack propagation in the weak layer was determined by analyzing the data from the geophones. The assumption was made that the fracture in the weak layer propagates radially outward from the point of initiation, and that the surface displacement travels at the same velocity as the fracture through the weak layer.

4 CONTRASTING WHUMPFIS AND REMOTELY TRIGGERED AVALANCHES WITH AVALANCHES NOT REMOTELY TRIGGERED

4.1 Introduction

The optimum way to gain the most information about whumpfs and remotely triggered avalanches is to collect field data from locations where these events have occurred. Due to the rare and unpredictable nature of whumpfs and remotely triggered avalanches only a limited number of events can be investigated each year. Over the past four years data have been collected at the sites of forty whumpfs and thirteen remotely triggered avalanches. In addition to collecting data from remotely triggered avalanche sites data have also been collected at the sites of fifty-two, human-triggered, dry slab avalanches that were skier triggered, but not remotely triggered. These two data sets are compared in this chapter to identify differences in the snowpack characteristics between remotely triggered avalanches and non-remotely triggered avalanches. In this chapter whumpfs are included with remotely triggered avalanches.

4.2 Variables

The data collected at sites of whumpfs and remotely triggered avalanches can be divided into three classes. Characteristics of the weak layer; characteristics of the overlying slab; variables that relate to both the weak layer and the overlying slab.

The first class of variables includes: age of the weak layer, thickness of the weak

layer, maximum crystal size of the weak layer, minimum crystal size of the weak layer, shear strength of the weak layer and temperature of the weak layer. The second class of variables includes: thickness of the overlying slab, overall slab density, the amount of load applied on the weak layer by the slab and the average hand hardness of the overlying slab.

The third class of variables relate to both the weak layer and the overlying slab. These data include stability and strength tests. The variables in the third class are: average compression test score, height of the snow pack, average rutchblock score, and a calculated stability index.

4.3 Data for Whumpfs and Remotely Triggered Avalanches

Before the classes of data are compared, they are tested for normality (Table 4.1). The Shapiro-Wilk test for normality is used (Shapiro et al., 1968, p. 1412). The hypothesis of normality is rejected at the 1% level ($p < 0.01$) for eleven of these variables. Of the thirteen variables for whumpfs and remotely triggered avalanches only the shear strength, slab density, rutchblock score and stability index can be considered normally distributed.

| <i>Table 4.1 Normality test for data collected at whumpfs and remotely triggered avalanches</i> | | | | | |
|---|--|-------------|-----------|---------------------------------|-------------------|
| Variable | | Mean | N | Shapiro- Wilk Test ¹ | |
| | | | | W | p |
| Weak-layer properties | Weak layer age (days) | 19.4 | 53 | 0.9407 | <10 ⁻⁵ |
| | Weak layer thickness (mm) | 3.6 | 45 | 0.499 | <10 ⁻⁵ |
| | Maximum crystal size (mm) | 10.1 | 49 | 0.882 | <10 ⁻⁵ |
| | Minimum crystal size (mm) | 5.3 | 53 | 0.889 | 0.001 |
| | Shear strength (kPa) | 0.76 | 38 | 0.934 | 0.028 |
| | Weak layer temperature(C) | -3.9 | 39 | 0.889 | 0.001 |
| Slab properties | Slab thickness (cm) | 63 | 53 | 0.927 | 0.002 |
| | Slab density (kg/m³) | 148 | 48 | 0.957 | 0.077 |
| | Load on weak layer (kPa) | 0.97 | 48 | 0.822 | 0.000 |
| | Average slab hardness (kN/m ²) | 13.3 | 53 | 0.908 | 0.000 |
| Stability indices | Compression test score | 15.8 | 40 | 0.917 | 0.006 |
| | Stability index | 0.81 | 38 | 0.964 | 0.251 |
| | Rutchblock score | 4.1 | 15 | 0.848 | 0.016 |
| | Height of snowpack (cm) | 178 | 53 | 0.922 | 0.002 |

¹ Rows for which $p \geq 0.01$ are marked in bold.

4.4 Data for Non-Remotely Triggered Avalanches

Similarly, the data for non-remotely triggered avalanche are tested for normality using the Shapiro-Wilk test in Table 4.2. The hypothesis of normality is rejected at the 1% level ($p \leq 0.01$) for eleven of the fourteen variables. Weak layer temperature, rutchblock score and stability index can be considered normally distributed data.

4.5 Contrast of Remotely Triggered Avalanches to Avalanches that were not Remotely Triggered

4.5.1 Introduction

A comparison between remotely triggered avalanches with avalanches not remotely triggered is done using fourteen variables. Twelve of these variables are easily measured in the field. The remaining two variables are indices that are calculated from the measured field data.

4.5.2 Comparison of Field Measured Variables

The following twelve variables are easily measured in the field: weak layer age, weak layer thickness, maximum crystal size, minimum crystal size, shear strength of the weak layer, weak-layer temperature, slab thickness, slab density, load on the weak layer, compression test score, rutchblock score and height of snowpack. These twelve variables are all not normally distributed for both remotely triggered avalanches and avalanches not

| Variable | | Mean | N | Shapiro- Wilk Test ¹ | |
|-----------------------|--|-------------|-----------|---------------------------------|-------------------|
| | | | | W | p |
| Weak layer properties | Weak layer age (days) | 10.9 | 22 | 0.815 | 0.001 |
| | Weak layer thickness (mm) | 0.9 | 40 | 0.592 | <10 ⁻⁵ |
| | Maximum crystal size (mm) | 4.3 | 46 | 0.804 | <10 ⁻⁵ |
| | Minimum crystal size (mm) | 2.5 | 49 | 0.674 | 0.001 |
| | Shear strength (kPa) | 0.62 | 39 | 0.894 | 0.002 |
| | Weak layer temperature (°C) | -4.4 | 35 | 0.946 | 0.085 |
| Slab properties | Slab thickness (cm) | 43 | 51 | 0.927 | 0.002 |
| | Slab density (kg/m ³) | 127 | 41 | 0.861 | <10 ⁻⁵ |
| | Load on weak layer (kPa) | 0.63 | 41 | 0.912 | 0.004 |
| | Average slab hardness (kN/m ²) | 5.4 | 43 | 0.664 | <10 ⁻⁵ |
| Stability indices | Compression test score | 15.4 | 38 | 0.970 | 0.384 |
| | Stability index | 0.77 | 38 | 0.953 | 0.110 |
| | Rutchblock score | 3.8 | 14 | 0.890 | 0.080 |
| | Height of snowpack (cm) | 178 | 53 | 0.922 | 0.002 |

¹ Rows for which $p > 0.01$ are marked in bold.

remotely triggered, and therefore require a comparison test that does not rely upon the distributional properties of the data. The variables are compared using the Mann-Whitney U test. The U test is designed to test for differences in the location between two populations (Neave and Worthington, 1988 p. 143) and is virtually as powerful as the *t*-test. In this test, the variables are arranged in rank order. The sums of the ranks for the two separate samples; R_1 and R_2 , are calculated the sample sizes for these are N_1 and N_2 respectively. The calculated the U statistic (Mann and Whitney, 1947) is

$$U = N_1 N_2 + \frac{N_1(N_1 + 1)}{2} - R_1 \quad (4.1)$$

A significant difference exists between the two samples when the *p* value is less than 0.05. Table 4.3 shows comparison of the twelve variables that are not normally distributed for both cases.

This analysis indicates that eight of the twelve variables show significant differences between remotely triggered avalanches and avalanches not triggered remotely. Additionally the Kolmogorov-Smirnov method (Neave and Worthington, 1988 p. 149) , another non-parametric comparison, was used to analyze the twelve non-normally distributed variables for general differences in population from which the samples were taken. Results, shown in Appendix A, also indicate significant differences in the same eight variables.

| <i>Table 4.3 Comparison of non-normally distributed variables using the U test</i> | | | | |
|--|-----------------------------------|---------------------------------------|--------------------------------------|--------------------------|
| Variable | Rank Sum Remotely Triggered | Rank Sum Non-Remotely Triggered | Calculated Statistic ¹ | |
| | | | <i>U</i> | <i>p</i> |
| Weak layer age | 1681.0 | 530.0 | 277.0 | 0.004 |
| Weak layer thickness | 2420.0 | 1235.0 | 415.0 | 1x10⁻⁵ |
| Maximum crystal size | 2912.5 | 1647.5 | 566.5 | 1x10⁻⁵ |
| Minimum crystal size | 3405.5 | 1950.5 | 725.5 | 1x10⁻⁵ |
| Shear strength | 1663.0 | 1340 | 560.0 | 0.065 |
| Weak layer temperature | 1586.5 | 1188.5 | 558.5 | 0.179 |
| Slab thickness | 3616.5 | 2054.5 | 728.5 | 1x10⁻⁵ |
| Slab density | 2553.0 | 1452.0 | 591.0 | 0.001 |
| Load on weak layer | 2532.0 | 1473.0 | 612.0 | 0.002 |
| Compression test score | 1584.5 | 1496.5 | 755.5 | 0.964 |
| Height of snowpack | 2007.0 | 3664.0 | 467.0 | 1x10⁻⁵ |
| Rutchblock score | 228.5 | 206.5 | 101.5 | 0.879 |

¹Rows for which $p \leq 0.05$ are marked in bold.

4.5.3 Comparison of Stability Index

Of the fourteen variables, only the stability index, was normally distributed for both sets of data. The stability index is a variable that is calculated using the shear strength of the weak layer, the load of the overlying slab and adjustment for ski penetration into the overlying slab (Jamieson and Johnston, 1998). This variable will be

compared using the two tailed T -test.

$$T = (\bar{u}_1 - \bar{u}_2) / (s_1^2 / n_1 + s_2^2 / n_2)^{1/2} \quad (4.2)$$

Where n_i is the sample size and s_i is the standard deviation of the sample. The null hypothesis is that there is no difference in the stability index. The probability that there is no difference between the two sample sets is p . The calculated T value is -0.47 with a p value of 0.64. The null hypothesis is accepted. There is no significant difference between the stability index measured at remotely triggered avalanches and the stability index measure at avalanches not remotely triggered.

4.5.4 Comparison of Average Slab Hardness

The hand hardness for each individual layer was measured in the field. The index values were then converted to more representative hardness values based on the measured areas of hand (Geldsetzer and Jamieson, 2000). The average slab hardness was not normally distributed for both data sets (Table 4.1 and 4.2) and is compared using the Mann-Whitney U test. The rank sum for remotely triggered avalanches was 3095. The rank sum for avalanches not remotely triggered was 1091. The calculated U statistic is 350.0 with a p -level of less than 10^{-5} . This indicates a significant difference of the average slab hardness between remote avalanches and avalanches not remotely triggered. Remotely triggered avalanches have slabs with mean hand hardness of 1F while avalanches not remotely triggered have slabs with an mean hand hardness of 4F+.

4.6 Weak Layer Crystal Type for Remote and Non-Remotely Triggered Avalanches

A marked difference exists between the crystal types of weak layers involved in remotely triggered avalanches and crystal types of weak layers involved in non-remotely triggered avalanches. Figure 4.1 shows the crystal types of weak layers for remotely triggered avalanches and avalanches not remotely triggered. Ninety-six percent of remotely triggered avalanches investigated occurred on weak layers consisting of facets, surface hoar, or depth hoar. All of these are considered persistent weak layers.

One of the two cases where field workers reported the failure on a non-persistent layer of decomposed and fragmented snow crystals, occurred on March 15, 2000. The failure originated in a layer approximately 4 cm above a crust, and traveled 1-2 meters before releasing several blocks near a roll. No facets were reported at the fracture site, but only 0.5 meters away faceted crystals were found near the crust. Field workers reported that the layer of facets could have contributed to failure in this remotely triggered avalanche. This leaves only one investigated whumpf or remotely triggered avalanche that did not occur on a persistent weak layer. Decomposed and fragment particles are the most common failure layer for non-remotely triggered avalanches that were investigated. Only forty-nine percent of avalanches not remotely triggered occurred on persistent weak layers.

The weak layer crystal types for remotely triggered avalanches were compared to weak layer crystal types for non-remotely triggered avalanches. The Pearson Chi-square is the most common test for significance of the relationship between two categorical variables (Neave and Worthington, 1988 p. 232). The calculated Chi-square statistic is

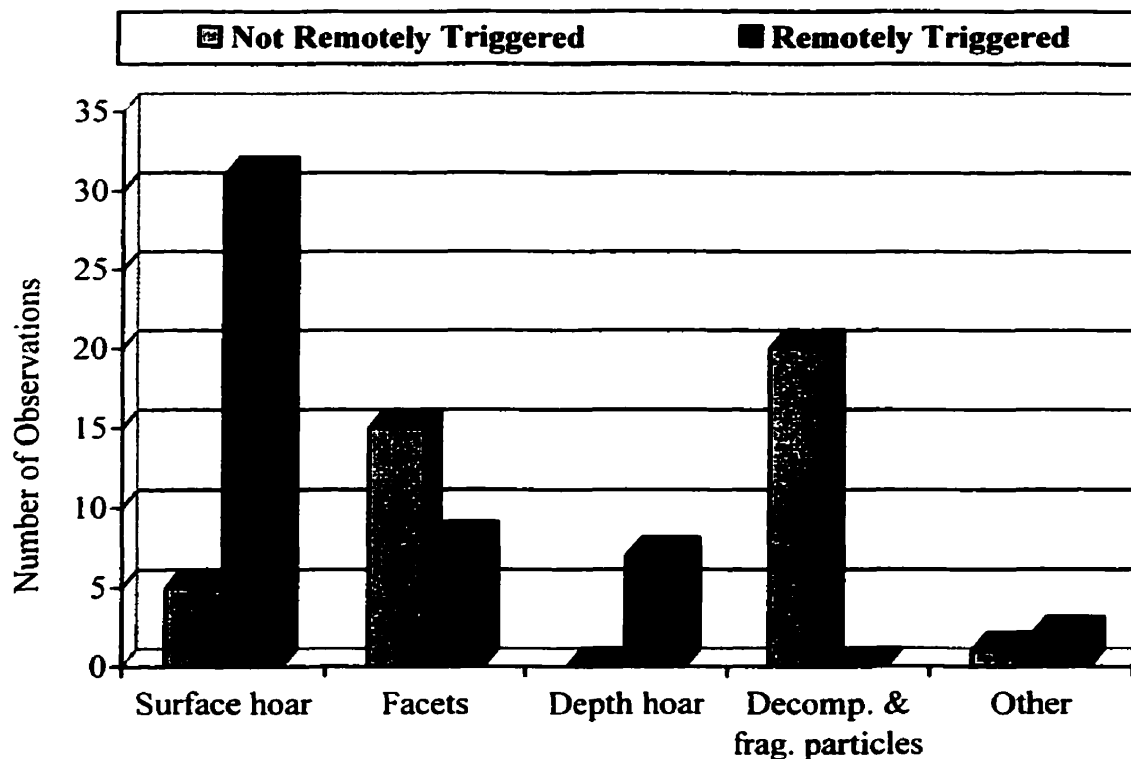


Figure 4.1 Comparison of the weak layer crystal types for remotely triggered avalanches and avalanches not remotely triggered.

29.02 with a significance level of 10^{-5} . This indicates that there is a significant difference in the weak layer crystal types for remote and non-remotely triggered avalanches.

The data collected from non-remotely triggered avalanches are biased towards persistent weak layers, i.e. facets, surface hoar and depth hoar. This is due to a concurrent research project that focuses on persistent weak layers, resulting in an exaggerated number of avalanches not remotely triggered occurring on persistent weak layers. Even though this bias existed the data still show a significant difference in the weak layer crystal type. Had this bias not existed in the data set a stronger significant difference would have been expected.

4.7 Discussion of Differences Between Remotely Triggered and Non-Remotely Triggered Avalanches.

The following conclusions can be drawn about the differences between avalanches that are remotely triggered and avalanches that are not remotely triggered. Compared to avalanches triggered from avalanche start zones, remotely triggered avalanches tend to:

1. Occur on older weak layers.
2. Have thicker weak layers.
3. Have weak layers with larger crystals.
4. Have slabs that are thicker
5. Have slabs with higher bulk density
6. Have slabs with a higher average hand hardness.
7. Have slabs that apply more static load on the weak layer.
8. Occur almost always on persistent weak layers.
9. Occur in areas with a shallower snowpack.

These differences are summarized in Table 4.4.

One possible explanation for these significant differences between remotely triggered avalanches and avalanches not remotely triggered is that the mechanism responsible for failure could be different. Schweizer (1999) states that while there are many plausible explanations for the failure initiation, there is still a lack of

| <i>Table 4.4 Variables that showed significant differences</i> | | | | |
|--|---|--------|-----------------------------------|--------|
| | Whumpfs and remotely triggered avalanches | | Not remotely triggered avalanches | |
| | N | Median | N | Median |
| Weak layer age (days) | 44 | 14.0 | 22 | 10.5 |
| Weak layer thickness (mm) | 45 | 1.30 | 40 | 0.50 |
| Maximum crystal size (mm) | 49 | 8.0 | 46 | 2.0 |
| Minimum crystal size (mm) | 54 | 3.0 | 49 | 2.0 |
| Slab thickness (cm) | 55 | 60.0 | 51 | 38.0 |
| Slab Density (kg/m ³) | 48 | 143 | 41 | 122 |
| Load on weak layer (kPa) | 48 | 0.76 | 41 | 0.54 |
| Height of snowpack (cm) | 55 | 147.0 | 51 | 300.0 |
| Average Slab hardness (kN/m ²) | 53 | 10.7 | 43 | 2.3 |
| Weak layer crystal type ¹ | 53 | SH | 51 | DF |
| ¹ Surface hoar (SH), Decomposed and Fragmented Particles (DF) | | | | |

comprehensive knowledge of the avalanche release process. He points out that macro scale fracture propagation experiments in the field are necessary.

Additional information indicating that a different failure mechanism might be responsible for whumpfs and remotely triggered avalanches is that eleven whumpfs or remotely triggered avalanches have been investigated with slope angles equal to or less than ten degrees, with seven of those occurring on horizontal terrain. Generally, dry slab avalanches are thought to occur rarely on slopes with an angle of less than twenty-five degrees (e.g. Perla, 1977). The fact that these whumpfs and remote failures occur on horizontal terrain contradicts one of the most widely accepted avalanche release mechanisms, which is shear fracture propagating through the weak layer and then failure of the flanks, crown and stauchwall. For slopes with inclination of less than twenty five

degrees, the shear stress and shear deformation in the weak layer are apparently not large enough to cause failure and fracture. This leads to the following hypothesis. The failure mechanism for whumpfs and remotely triggered avalanches is different than the failure mechanism for non-remotely triggered avalanches. Comparing snowpack characteristics is one indirect way to test this hypothesis. The null hypothesis is that the release mechanisms are the same, and the alternative hypothesis is that the release mechanisms are different. Several important snowpack characteristics showed significant differences between remotely triggered avalanches and non-remotely triggered avalanches. This supports the alternative hypothesis that the release mechanism is different for remotely triggered avalanches and whumpfs.

A theory will be developed in Chapter 6 that will help to explain these differences and show why certain snowpack characteristics might be necessary before a whumpf or remotely triggered avalanche can occur.

5. Propagation Measurements and Cantilever Beam Tests at Sites of Whumpfs and Remotely Triggered Avalanches.

5.1 Introduction

Measurements of propagation distance and fracture speed were made at the sites of some whumpfs and remotely triggered avalanches. In addition, cantilever beam tests were performed at the sites of eight whumpfs. The resulting data help to understand fracture propagation better and are used to develop a theory for fracture propagation through a horizontal snowpack in Chapter 6.

During the winter of 1999/2000, when extent of weak layer fracture could be determined, thickness measurements were made of the fractured and unfractured weak layer. These measurements were used to calculate the change in thickness of the weak layer. In the spring of 2000 geophysical instrumentation was used to measure the velocity of a fracture propagating through a weak layer in the snowpack.

5.2 Propagation Distance of Weak Layer Fractures

The propagation distance was measured or estimated at sites of thirty-five whumpfs and at the sites of fourteen remotely triggered avalanches. The distances ranged from 1 m to 300 m. The data for whumpfs are summarized in Figure 5.1, showing that most of the whumpfs propagated less than 20 m with four extreme events

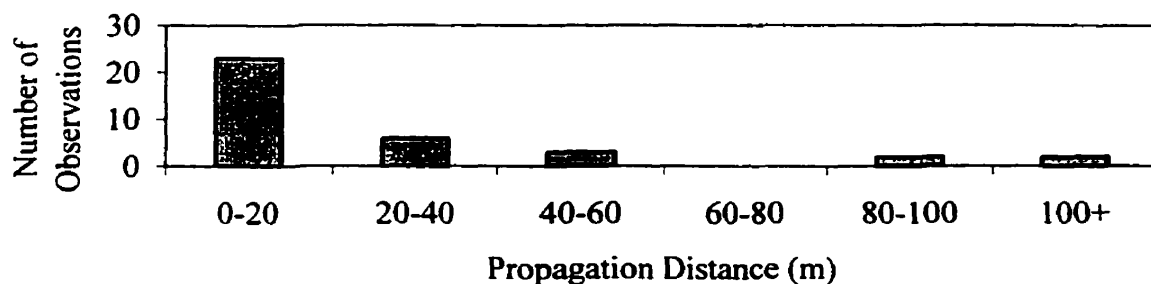


Figure 5.1 Weak layer fracture propagation distance at whumpf sites.

that propagated greater than 80 m. Eleven of these whumpfs occurred on slopes of less than ten degrees, with the furthest propagation occurring on a slope less than ten degrees being 100 m.

The propagation distances for remotely triggered avalanches are shown in Figure 5.2. Remotely triggered avalanches show a greater propagation distance compared to whumpfs. The distances range from a minimum of 20 m to a maximum of 300 m. Half of the fourteen remotely triggered avalanches investigated propagated over 100 m. The slope angle, where the slab avalanche was released, ranged from 28° to 55°

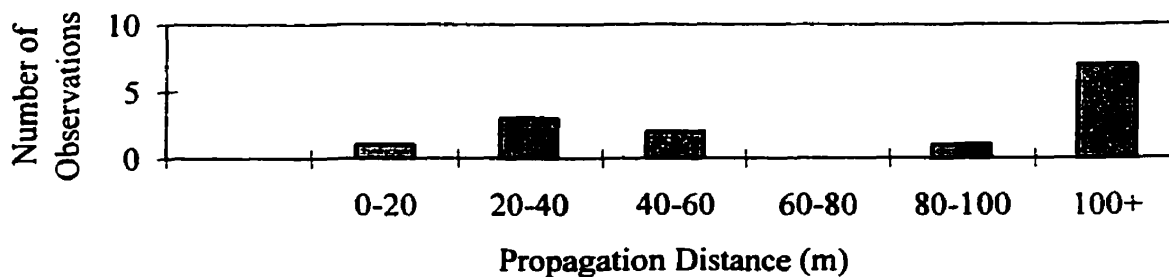


Figure 5.2 Weak layer fracture propagation distance at remotely triggered avalanche sites.

degrees with the furthest propagation distance of 300 m occurring on the steepest slope of 55°.

5.2.1 Sources of Error for Propagation Distance Measurements

Measuring the distance that fractures propagated in weak layers was challenging. The extent of propagation for remotely triggered avalanches was considered to be the distance from the location of the trigger to the perimeter of the released slab avalanche. It is certain that the fracture through the weak layer propagated this minimum distance. The actual furthest extent of propagation is unknown.

The extent of propagation for whumpfs was easier to determine. During the winter of 1999/2000 the extent of propagation was determined at five of eight investigated whumpfs. This extent was determined by either visually finding a perimeter crack on the surface or by observing the motion of the vegetation protruding through the surface. Often the fracture stopped where the slope angle changed or at a terrain feature such as a tree.

5.2.2 Fracture Propagation Stopping Condition

With the limited amount of available arrest data the only conclusion that can be drawn about fracture propagation through weak layers is that it often stops at terrain features. These include changes in slope angle (concavities or convexities) and vegetation protruding through the surface of the snow. Similar to crown fractures for slab avalanches, the perimeter cracks delineating the fractured area in a whumpf often

connect trees and bushes protruding through the surface (e.g. McClung and Schaerer, 1993, p. 102).

5.3 Change in Thickness of the Weak Layer

During the winter of 1999/2000 the change in thickness of weak layers before and after fracture was measured at the sites of five whumpfs. It is often difficult to predict when or where a whumpf will occur so it becomes impractical to make measurements prior to a whumpf occurring. Instead of taking

measurements prior to the fracture, two measurements are made after a whumpf occurs when the extent of propagation is known. The first measurement is of the thickness of the weak layer where it has fractured, usually near the trigger point. The second measurement is the thickness of the weak layer where it has not fractured. This second measurement is used as the thickness of the weak layer prior to fracture. In some cases the displacement of the weak layer can be measured by the vertical displacement of the snow's surface. This occurs when a perimeter crack is visible at the edge of the fractured weak layer (Figure 5.3). The



Figure 5.3 Perimeter crack of a whumpf showing surface displacement (3-4 mm) corresponding to collapse of the weak layer. Bow Summit, Banff National Park, ASARC photo.

Table 5.1 Thickness of weak layer before and after a whumpf.

| Date | Weak Layer (WL) crystal type | Crystal size (mm) | WL depth (cm) | WL thickness (mm) | Fractured WL thickness (mm) | Change in WL thickness (mm) |
|----------|---------------------------------|-------------------------|---------------------|-------------------------|-----------------------------------|--------------------------------------|
| 00-01-06 | Surface hoar | 12-25 | 37.0 | 29.6 | 26.8 | -2.8 |
| 00-01-06 | Surface hoar | 10-15 | 65.0 | 15.0 | 12.0 | -3.0 |
| 00-01-07 | Surface hoar | 10-20 | 40.0 | 22.0 | 12.0 | -10.0 |
| 00-01-31 | Surface hoar | 6-8 | 39.5 | 9.0 | 7.0 | -2.0 |
| 00-02-19 | Surface hoar | 3-7 | 39.0 | 14.0 | 13.2 | -0.8 |

number of measurements is also limited because it is often difficult to determine where fracture propagation in the weak layer stopped. At several whumpf sites, a crack originating from the tip of the weak layer fracture extended to the surface. This visibly delineated the area where the weak layer fractured. Table 5.1 shows the cases where thickness measurements could be performed. All five cases, where the measurement could be performed, showed a decrease in the thickness of the weak layer. The average change in thickness was 3.7 mm with the smallest and largest change in thickness being 0.8 mm and 10 mm respectively.

5.4 Measurement of the Propagation Speed of Fracture through a Weak Snowpack Layer

5.4.1 Location and Description of Experimental Setup

On 19 February 2000, the author along with several staff from the University of



Figure 5.4 Experimental setup to record fracture propagation velocity. Bow Summit, Banff National Park, ASARC photo.

Calgary Applied Snow and Avalanche Research Group successfully triggered and measured the velocity of a propagating fracture in a buried weak snowpack layer. The experiment took place at Bow Summit, Banff National Park, Alberta, Canada. Several days prior to the experiment, whumpfs had been reported to be occurring on a widespread basis in this area. Upon arriving in the area, this was confirmed by triggering several whumpfs while walking on snowshoes through several open meadows. At an undisturbed site, a string of six geophones spaced approximately 5 m apart were laid in a line across the site on the surface of the snow (Figure 5.4). These were connected to a Bison 9000 Series Digital Seismograph, sampling at 2000 Hertz with 0 db gain. Positioning the geophones without disturbing the site required walking around the perimeter of the meadow and then pulling the geophones into place using a

load-bearing rope. Triggering a whumpf after positioning the geophones took about nine attempts over three days.

5.4.2 Snow Conditions

The weak layer that fractured was 0.4 m below the surface and approximately 10 mm thick. It was composed of surface hoar crystals, ranging in size from 3 mm to 7 mm, that had formed during a cold clear period approximately fifty days prior to the experiment date. The overlying slab had an average density of 189 kg/m^3 with lower density layers near the surface and higher density layers (240 kg/m^3) closer to the weak layer.

5.4.3 Observations and Results

The Bison recorder was capable of recording six channels at 2000 samples per channel per second for 20 seconds. After the recorder was triggered a person on snowshoes loaded the snowpack near the end of the geophone string by walking in a small area, in an attempt to trigger a whumpf. A whumpf was triggered and each geophone recorded vertical displacement of the snow's surface as the fracture traveled beneath. The geophone trace (Figure 5.6) clearly shows the arrival of the fracture with a large signal generated from the vertical displacement of each geophone. The trace also indicates that the propagating fracture did not reach the furthest two geophones from the recorder. This indicates that the fracture propagated between 12.7 and 17.4 meters. There was no visible perimeter crack on the surface of the snow. Measurements of the

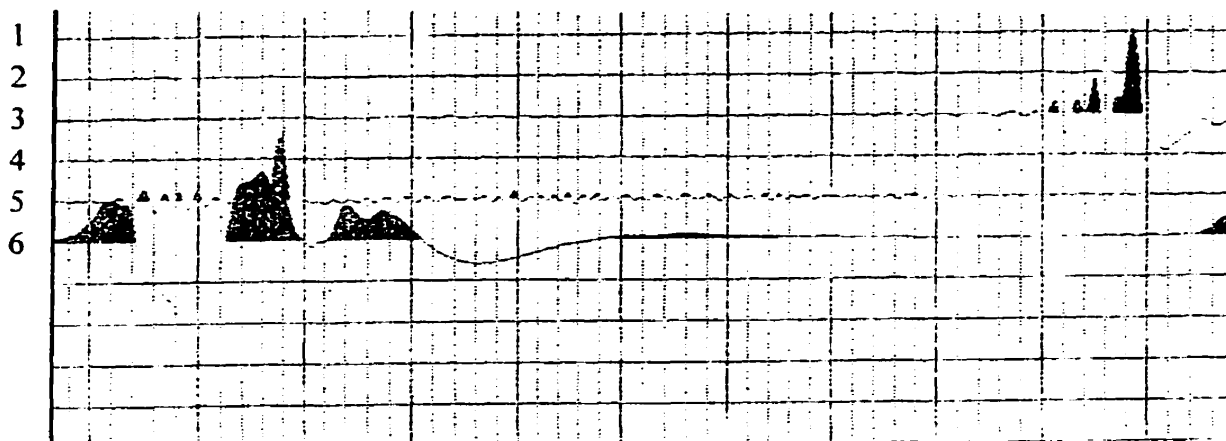


Figure 5.5 Signal traces produced by the Bison recorder indicating the time of arrival for fracture in the weak layer. Vertical lines represent 10 ms.

weak layer thickness showed a collapse of approximately 1 mm.

Table 5.2 shows the distance between the trigger point and each geophone, and the arrival time of the surface displacement associated with the fracture of the weak layer. The velocity of the propagating fracture was then calculated between third and fifth geophone using the distance from the trigger to each geophone and the arrival time. This velocity was calculated to be 19.9 m/s. The calculated velocity between geophones

Table 5.2 Distance from whumpf trigger point to each geophone, with arrival time of surface displacement.

| Geophone Number | Distance From Trigger Point to Geophone (m) | Arrival Time (milliseconds after triggering recorder) |
|-----------------|---|---|
| One | 21.30 | No arrival |
| Two | 17.40 | No arrival |
| Three | 12.70 | 7690 |
| Four | 9.00 | (defective geophone) |
| Five | 4.75 | 7290 |
| Six | 2.65 | 7200 |

3 and 6 was 20.5 m/s and the calculated velocity between geophones 5 and 6 was 23.9 m/s.

5.4.4 Discussion

This was the first time that the velocity of a fracture propagating through a weak snow pack layer has been measured. In addition to measuring the velocity, detailed snowpack information was also collected, including shear strength of the weak layer and stability test results for the slab-weak layer combination.

In calculating the velocity, two assumptions were made. The first is that the vertical displacement of the snow surface travels at the same velocity as the fracture through the weak layers. The second assumption was that fractures in the weak layer originate at one point and propagate outwards in two dimensions. These two assumptions were originally proposed by Lackinger in 1989. He stated that one failure mechanism could be that the weak layer fails in compression and that an area of bending in the overlying slab widens outward from the initial failure. The measured velocity lies within the two estimated values for fracture propagation through a weak layer of 6 m/s and 300 m/s. The estimated value of 6 m/s was through snow that was isothermal (Truman, 1973), while the estimated value of 300 m/s was in cold dry snow in Antarctica with a thick hard overlying slab (DenHartog, 1982).

The measured velocity of 20 m/s and the estimated velocity of 6 m/s by Truman are much slower than would be expected for a Mode II brittle shear fracture in snow.

Bader and Salm (1990) propose that propagating shear fractures through weak layers in the snowpack would have velocities on the order of 100 to 1000 m/s. Gubler (1977) reported through experimentation that brittle fractures in the snowpack propagated at roughly half of the shear-wave velocity. His measurements did not include fracture through a weak layer. McClung (1979) states that the velocity of a shear fracture through

| Density | Logitudinal (m/s) | Shear Wave (m/s) |
|---------|-------------------|------------------|
| 210 | 500 | 229 |
| 250 | 625 | 375 |
| 300 | 1000 | 500 |
| 350 | 1166 | 708 |
| 410 | 1270 | 746 |
| 440 | 1312 | 758 |
| 508 | 1637 | 1085 |
| 551 | 2225 | 1265 |
| 600 | 2518 | 1321 |

From Smith (1965)

a weak layer would be 1/2 the shear wave velocity of the snow directly above the weak layer. The measured density of the snow above the weak layer on February 19th was 246 kg/m³. The longitudinal and shear wave velocity can be interpolated from measured wave propagation velocities in snow as presented in Table 5.3. Using the density of the snow directly above the weak layer and McClung's (1979) assertion, yields a value of 170 m/s, considerably higher than the value measured on February 19th.

Fracture mechanics texts (e.g. Broek, 1986) indicate that a component of shear or tension is necessary for fracture propagation. A hypothesis that fractures propagating through weak layers on horizontal terrain require a compressive component is discussed

in Chapter 6.

5.5 Cantilever Beam Tests

5.5.1 Introduction

The cantilever beam test has been used in three previous studies to test the flexural strength of snow (Perla, 1969; Mears, 1998; Sterbenz, 1998). A new technique was developed that was capable of testing the slab overlying a weak layer as one unit. This technique used a new saw that facilitated a constant rate of cutting under the beam. The technique used by Perla and Mears did not undercut the cantilevered beam at a constant rate.

5.5.2 Variability and Number of Tests for Required Precision

During the winter of 1998/1999, 28 sets of cantilever beam tests were performed with the number of tests per set ranging from 3 to 30. A total of 190 tests were completed. The within-set coefficient of variation averaged for the 28 sets of tests was 7.8% with a maximum of 12.6% and a minimum of 2.0%. The largest set (30 tests) had a coefficient of variation of 9.9%. One noticeable trend was that the coefficient of variation improved with experience of the operator. The average for first six sets was 8.7% compared to 6.4% for the last six sets. From these data the appropriate sample size can be estimated for repeated tests on the same overlying slab.

On 9 January 2000, 30 cantilever beam tests were performed in one area to

precision of 15% from three repeated tests.
 test. With 90% confidence, the mean length of undercut can be determined with a
 Table 5.4 shows the number of tests for $v = 0.10$ which is typical for the cantilever beam

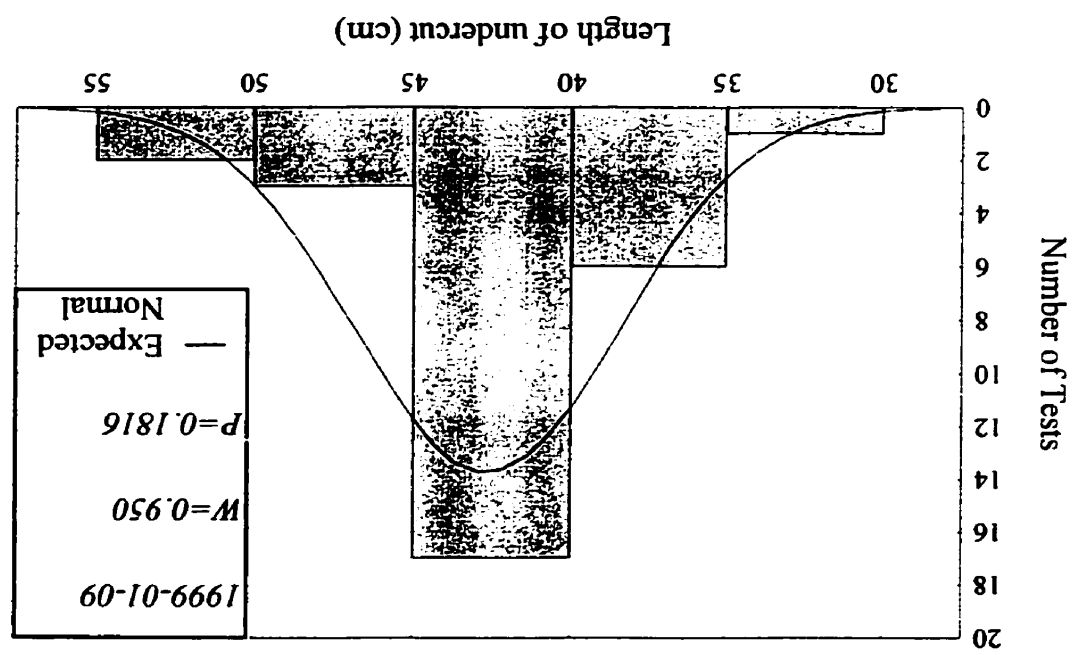
$$n = (T^{p:n-1} v / P)^2 \tag{5.1}$$

from the coefficient of variation, v , by solving

The number of tests, n , required to obtain precision, P , can be estimated
 be worthwhile.

beam test results are considered normally distributed. Further repeated set studies would
 normality cannot be rejected for this data set. In the following analysis, the cantilever
 normality. The calculated W value is 0.950 with a p -value of 0.182. The hypothesis for
 these data are presented in Figure 5.6. The Shapiro-Wilk test is used to test the data for
 determine if the test results can be considered normally distributed. The distribution of

Figure 5.6 Frequency distribution for the set of 30 cantilever beam tests.



| Required Precision of mean, P % | Confidence level, $1-2\alpha$ % | Estimated number number of tests, n |
|---------------------------------------|---------------------------------------|--|
| 10 | 90 | 5 |
| 10 | 95 | 6 |
| 15 | 90 | 3 |
| 15 | 95 | 4 |

5.5.3 Correlation Between Calculated Beam Number and Average Slab Density

An average beam number for each set of tests was calculated using the formula (Eq. 2.1) developed by Perla (1969). The beam number can be considered an index for the flexural strength of the overlying slab. It is the calculated tensile stress at the top of the beam, assuming the beam behaves as a homogenous and linear elastic material. Since beams of natural snow are rarely homogenous and the fracture may not start in the intergranular bonds at the top of the beam, the beam number is considered an *index* of flexural strength rather than a measure of the tensile strength (Perla, 1969). The average beam number is plotted against the bulk density of the slab on semi-log scale in Figure 5.7. The calculated beam number correlated well with overall slab density measurements. These tests were performed for beams 25 and 50 cm thick.

The limits from Perla (1969) are also plotted on Figure 5.7. The results show less scatter than most strength studies of snow (Shapiro et al., 1997). The following factors could have contributed to these consistent results. The beams were undercut at a constant

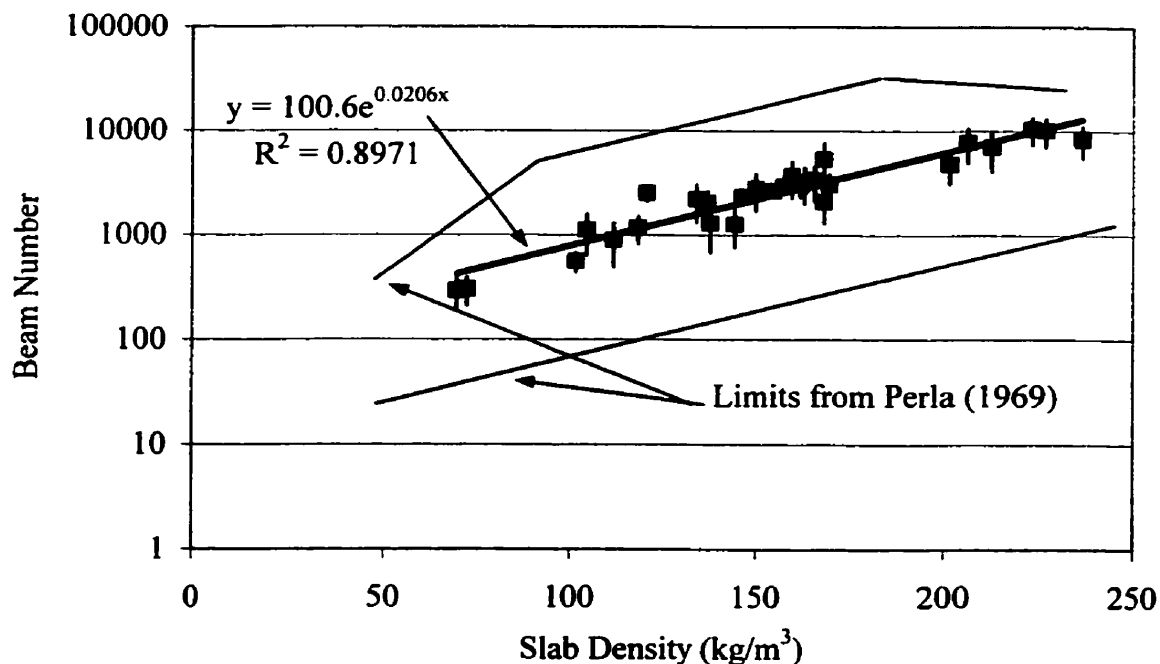


Figure 5.7 Cantilever beam tests performed for beams, 25 cm and 50 cm thick. Error bars represent one standard deviation.

rate and the sides of the beams were cut, with a 130 cm snow saw, to minimize imperfections and ensure consistent dimensions. The testing was also limited to one operator.

Two unusual slabs were also tested in this study. The snowpack for these two slabs consisted of higher density snow layers above lower density snow layers, opposite to what is normally observed in the field. The results from these tests are consistent with the rest of the slabs tested. Consequently, for the limited range of slabs tested, no substantial effect of layering on the beam number was determined.

5.5.4 Qualitative Differences for Cantilever Beam Tests at Whumpfs

The cantilever beam test was performed at the sites of eight whumpfs during the winter of 1999/2000. The overlying slab was undercut along the weak layer to produce a cantilevered slab. These tests showed significantly different fractures than slabs tested with no weak layer present. When no weak layer was present the vertical fracture at the back of the beam was usually within 5 cm of the end of the undercut, and was surmised to start on the surface where tensile stress peaks and propagate downward to the undercut. At the eight whumpf sites where the undercut was along a weak layer the vertical fracture at the back of the beam was 30-60 cm beyond the end of the undercut, usually at the end of the excavated pit (Figure 5.8). The first visible fracture was in the weak layer and observed to start at the end of the saw cut and propagate through the weak layer. The fracture of the weak layer always ended at a near-vertical fracture in the slab. This fracture through the slab almost certainly started at the surface and propagated down through the slab because:

- the propagating fracture in the weak layer subjects the slab to bending, with

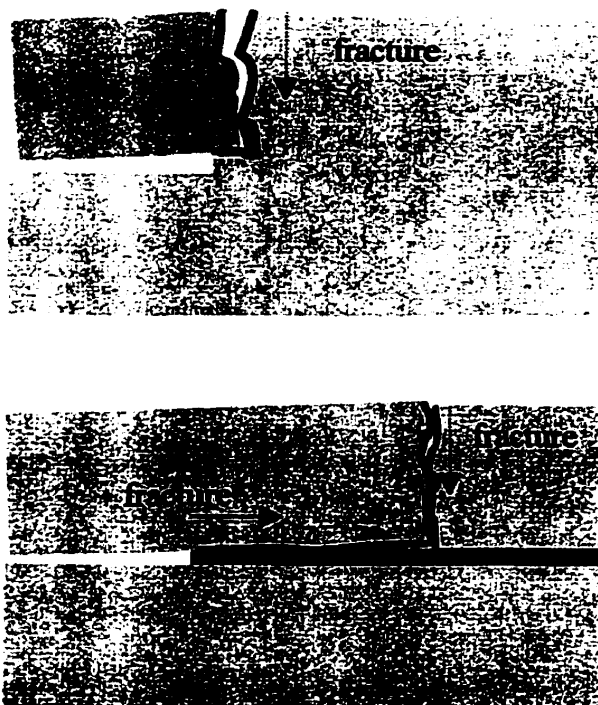


Figure 5.8 Cantilever beam fracture (above) typical fracture when no weak layer is present (below) typical fracture when a persistent weak layer being cut.

tensile stress at the surface and compressive stresses at the base of the slab near the weak layer;

- for a homogeneous slab, the fracture would start at the surface since the tensile strength of snow is less than the compressive strength; and
- snow slabs are almost always less dense and consequently less stiff and weaker at the surface than at their base.

Since the fracture in the weak layer was never observed to extend beyond the near-vertical fracture through the slab it is very likely that the fracture through the slab stops the fracture in the weak layer. This suggests that propagating fractures in weak layers would stop where the slab was locally weak or bending stresses increased at changes in slope angle such as where the slab was convex. Thus fracture propagation would be influenced by the variations in the bending strength of the slab as well as by the energy balance for fracture propagation. Where the slab is very uniform such as on lakes and level ground without vegetation, the propagation distances might be greater than where the slope angles varies and/or where the ground cover, vegetation or related snow metamorphism locally weakens the slab.

The cantilever beam test showed that the slab and weak layer combination fails substantially differently than when a slab was tested without an underlying weak layer present.

5.5.5 Quantitative Differences for Cantilever Beam Tests at Whumpfs

The cantilever beam tests performed at the sites of whumpfs also show

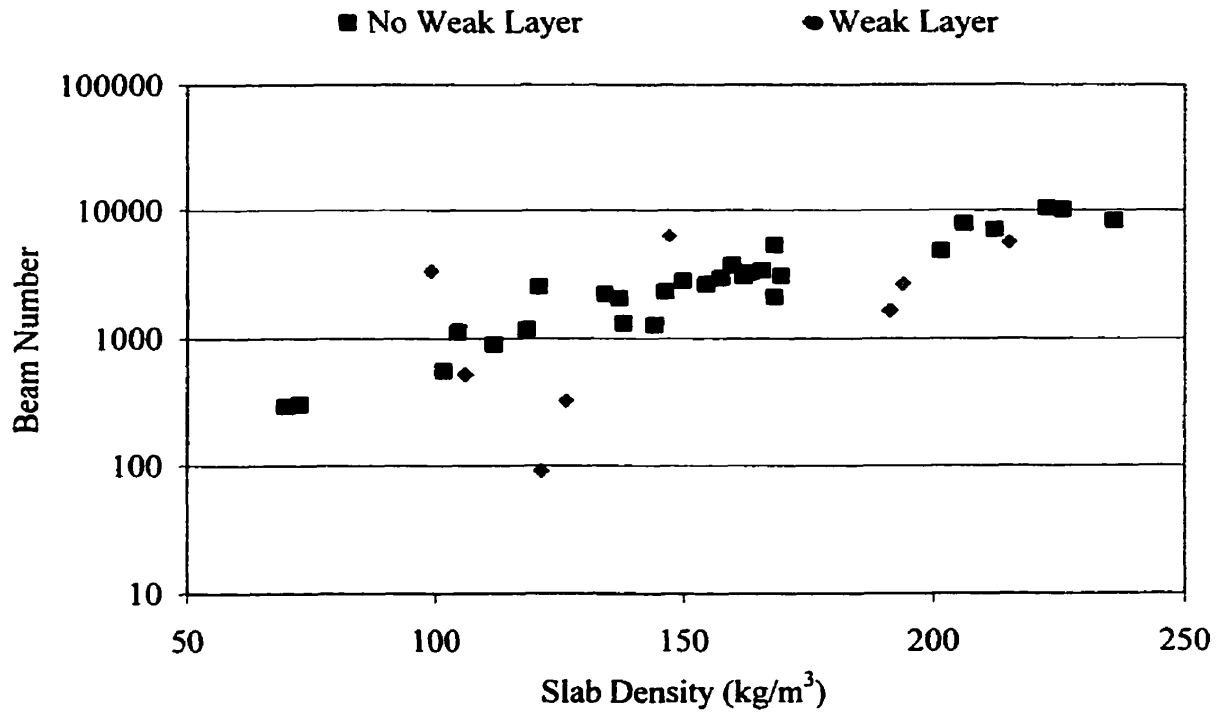


Figure 5.9 Cantilever beam tests performed at sites with and without weak layers.

quantitative differences from cantilever beam tests performed with no weak layer present. Figure 5.9 shows the results from cantilever beam tests performed at whumpf sites plotted with cantilever beam tests performed with no weak layer present. Cantilever beam tests at sites with weak layers show a much greater scatter when plotted against slab density than tests where no weak layer was present.

5.6 Conclusions

The data collected at sites of whumpfs and remotely triggered avalanches have helped to draw some specific conclusions about fractures in weak snowpack layers.

- The propagation distances were estimated at the sites of some investigated whumpfs and remotely triggered avalanches. The observations suggest that the stopping condition might be controlled by terrain.
- The speed of a propagating fracture through a weak layer was measured at 19.9 m/s. This was measured using geophysical instrumentation. The measured speed was much slower than the expected speed for a propagating shear fracture through a weak snowpack layer.
- The cantilever beam test was used to show that the slab weak layer combination performs differently than a slab without a weak layer present. When the overlying slab was cantilevered over a persistent weak layer the fracture started in the weak layer near the saw and propagated towards the root of the beam. It is argued that the vertical fracture in the slab stops fracture in the weak layer.

6 Theory for Weak Layer Fracture on Low-Angle Terrain

6.1 Introduction

This chapter introduces a theory for weak layer fracture propagation on low-angle terrain. It is the first theory that offers a plausible explanation for weak layer fracture propagation through low angle and horizontal terrain. In section 6.2 two existing theories for slab avalanche release are presented. These theories offer no explanation for fracture propagation of weak layer through horizontal terrain. Section 6.3 introduces the new theory and describes the two major components; a flexural wave in the overlying slab and fracture of the weak layer due to the bending of the overlying slab. The equations governing a flexural wave are developed in Section 6.4 and applied to snow conditions of 19 February 2000. Section 6.5 uses a comparison between the cantilever beam test and a flexural wave to show that the two could fracture the weak layer in a similar manner. Section 6.6 provides a brief discussion of energy associated with the propagation of a flexural wave coupled to the fracture of the weak layer. Whumpfs and remotely triggered avalanches are often associated with the sound that is heard when they are triggered. A discussion of how the sound is generated is presented in Section 6.7. Section 6.8 provides additional discussion of the theory.

It should be noted that this theory has been developed for failures on horizontal terrain that are triggered by an oversnow traveler and that on steeper terrain more traditional avalanche release mechanisms such as those discussed in Section 6.2 are most likely responsible for avalanche release.

6.2 Application of Previous Avalanche Release Theories to Whumpfs

Perla and LaChapelle introduced a theory for snow slab failure in 1970. They argued that shear strain in the weak layer leads to a crown fracture through the overlying slab and is followed by shear fracture of the weak layer. Their model focused on an inclined snowpack with a weak layer under a cohesive snow slab. The inability of the weak layer to sustain basal shear stress imposed by the slab and the ability of the weak layer to form a slip surface, result in an important increase in the maximum principal stress upslope from the slip surface in the overlying slab. If this tensile stress in the slab increases at a sufficient rate, brittle fracture may commence in the slab and propagate through the weak layer.

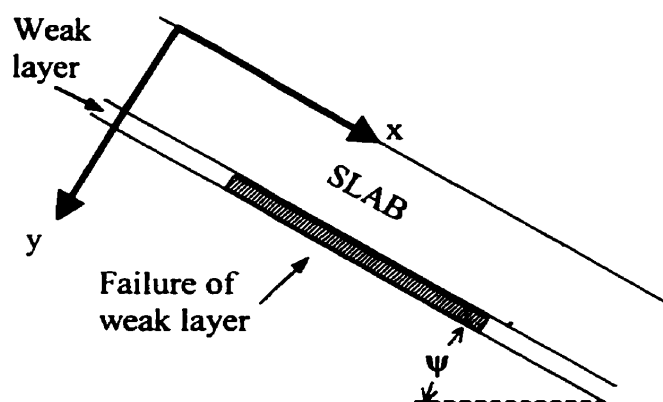


Figure 6.1 Model of slab avalanche failure. Hatched area indicates failure of the weak layer.

Critical to their analysis is the down slope component of shear stress from the slab induced on the weak layer to create a slip surface. The shear stress increase at the edge of the slip surface causes propagation of this slip surface. If this snow slab failure model is applied to a weak layer on horizontal terrain, there is no shear stress imposed on the weak layer. Therefore there would be no increase in shear stress at the edge of a slip surface; a slip surface would not propagate. The conditions for fracture of the slab followed by weak layer fracture would not be met.

McClung (1979) proposed a theory for slab avalanche initiation where shear fracture in the weak layer precipitated by strain softening leads to fracture in the weak layer followed by fracture of the overlying slab. McClung's theory is based on earlier work by Palmer and Rice (1973). They developed a theory for the initiation and growth of slip surfaces in narrow zones of overconsolidated clay; which they called these shear bands. McClung makes the assumption that snow in a weak layer acts like a shear band, and that the weak layer fails as it does in laboratory shear experiments. The basic premise behind his theory is that shear stress imposed by the overlying slab creates a shear band in the snowpack within a weak layer. A slow strain softening at the tip of the band follows, until a critical length is reached. The fracture then becomes brittle and propagates rapidly. The propagation velocity of the band would be limited to the order of one half the shear wave velocity in the body of the slab (McClung, 1979). Similar to Perla and LaChapelle (1970), McClung's model relies on gravitational force on the slab to provide shear stress in the weak layer. The shear stress concentration at the edges of a slip band due to gravitational forces is needed for crack propagation to occur.

The difference between these two theories is whether the initial fracture occurs in the weak layer or in the crown. Both theories predict that the initial *failure* would be in shear within a weak snow pack layer. When applied to horizontal terrain both theories fail to explain propagation of a shear fracture through a weak snowpack layer. Similar to these two theories all snowpack failure models to date have focused on inclined snowpacks (Schweizer, 1999) where gravitational forces exerted on the overlying slab produce shear stress in a weak snowpack layer.

It has been shown (Föhn, 1987) that a line load due to an oversnow traveler

causes shear stress in a weak layer on horizontal terrain. It is possible that this increase in shear stress could fracture a weak layer in a specific area, but the shear fracture would not propagate outside of an oversnow traveler's zone of influence. A mechanism other than gravitational forces on the slab, or shear stress induced by an oversnow traveler, is needed to provide the shear stress in the weak layer to propagate fractures large distances (>5 m) through horizontal terrain.

6.3 New Theory for Avalanche Initiation on Low-Angle Terrain

The following theory is presented to explain fracture propagation on low-angled terrain where the gravitational shear forces in the weak layer are negligible. This theory would apply to both whumpfs on low angled terrain, and remotely triggered avalanches that are initiated on low-angle terrain. This theory only deals with artificially triggered avalanches that arguably result from a different failure mechanism than avalanches occurring naturally (e.g McClung and Schaerer, 1993, p. 51).

The first event is a compressive fracture in the weak layer due to a force normal to the snow's surface. The compressive fracture in the weak layer results in the bending of the overlying slab. The slab is assumed to be fixed at the edges of the zone of compressive failure. The resulting moment in the overlying slab translates to shear stresses and strains in the connected weak layer near the edge of the collapsed zone. The weak layer then fractures in shear at the edge of this zone. The bending of the slab propagates outward from the initial trigger point, progressively fracturing the weak layer in shear. Fracture of the weak layer is coupled to the bending wave that propagates through the overlying slab (Figure 6.2). The speed of this system is governed by the

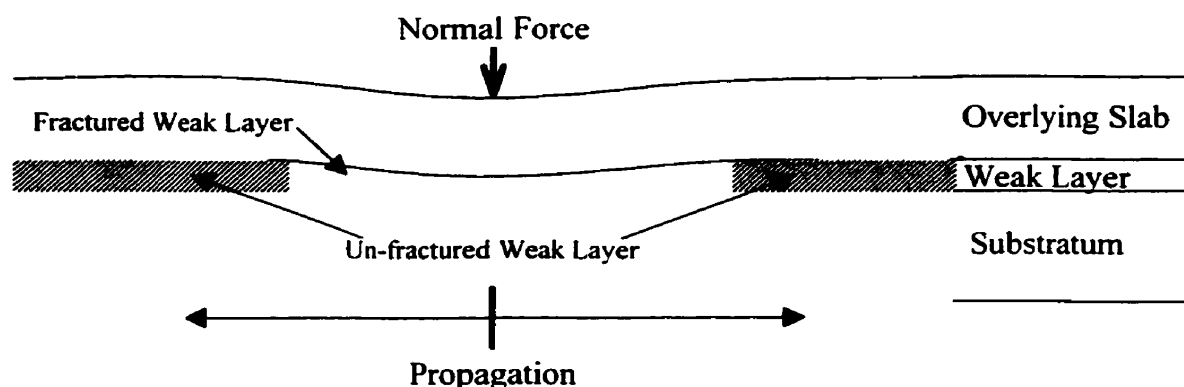


Figure 6.2 Schematic of the proposed theory for whumpfs and remotely triggered avalanches. The weak layer is initially failed in compression bending the overlying slab, which propagates shear fracture through the weak layer.

speed of the flexural wave that propagates through the overlying slab.

6.4 Flexural Waves Through the Overlying Slab

There are four basic waves that can propagate through solids; each propagates with a different velocity (Hueter and Bolt, 1955). The highest velocity is associated with bulk waves. The next highest is associated with longitudinal waves in a slender bar at low frequencies (wavelength much greater than diameter). Shear waves propagate with a still lower velocity. The lowest velocity occurs with flexural waves. The measured displacement downward of the overlying slab at the sites of investigated whumpfs, and the fact that this displacement originates at one point and propagates outwards much more slowly than the velocity for shear or longitudinal waves supports the idea that a flexural wave travels through the overlying slab. Wilson (1955) states that any disturbance of a floating ice sheet generates flexural waves in the ice. A slab overlying a weak layer can be thought of as a plate. Equally, any disturbance to this plate would also

produce a flexural wave through the plate. The fact that a sound is generated with the propagation of a whumpf also supports the fact that flexural wave travels through the overlying slab. Rossing and Fletcher (1995) report that flexural waves are associated with the radiation of sound, while longitudinal and shear waves do not produce significant sound.

The simplest theory for flexural waves in beams and plates is based on the Bernoulli-Euler theory for a beam (Graff, 1975). This theory yields a dispersive system. The velocity of a flexural wave is dependent upon the wavelength, which in turn is dependent on the flexural properties of the slab. As the flexural rigidity increases in a plate or beam, so to does the velocity of flexural waves.

In this section, a simple model of propagating flexural waves in a beam is developed based on work by Graff (1955). Consider a thin beam that undergoes a transverse motion (Figure 6.3a). Bending moment and shear forces act on each beam element (Figure 6.3b). If we assume that plane cross-sections initially perpendicular to the axis of the beam remain plane and perpendicular to the neutral axis during bending, then the relationship between the bending moment and curvature is given by

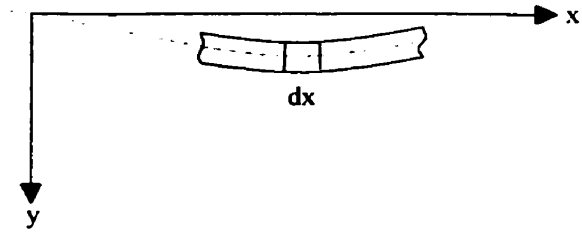


Figure 6.3a Beam undergoing transverse motion.

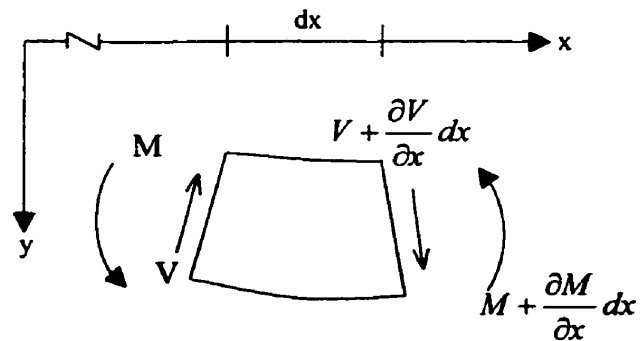


Figure 6.3b Bending and shear forces acting on a beam element.

$$\frac{\partial^2 y}{\partial x^2} = \frac{-M}{EI} \quad (6.1)$$

where y is the coordinate measured from the neutral surface of the beam, M is the moment and I is the moment of inertia. It is assumed that slopes and deflections of the beam are small. Writing the equation of motion in the vertical direction

$$-V + \left(V + \frac{\partial V}{\partial x} dx\right) = \rho A dx \frac{\partial^2 y}{\partial t^2} \quad (6.2)$$

where A is the cross sectional area of the beam, ρ is the mass density per unit volume and V is shear force. This equation then reduces to

$$\frac{\partial V}{\partial x} = \rho A \frac{\partial^2 y}{\partial t^2} \quad (6.3)$$

The next equation is the summation of moments for Figure 6.3b. Ignoring rotational inertia effects the moment equation is

$$V = \frac{\partial M}{\partial x} \quad (6.4)$$

Substituting equation 6.4 into 6.1 gives

$$\frac{\partial^2 M}{\partial x^2} = \rho A \frac{\partial^2 y}{\partial t^2} \quad (6.5)$$

and finally substituting equation 6.1 into equation 6.5 yields

$$\frac{\partial^2}{\partial x^2} \left(EI \frac{\partial^2 y}{\partial x^2} \right) + \rho A \frac{\partial^2 y}{\partial t^2} = 0 \quad (6.6)$$

as the governing equation for the transverse motion of a thin rod or beam. If E and I are constant Equation 6.6 reduces to

$$\frac{\partial^4 y}{\partial x^4} + \left(\frac{1}{a^2} \right) \left(\frac{\partial^2 y}{\partial t^2} \right) = 0 \quad \text{where} \quad a^2 = \frac{EI}{\rho A} \quad (6.7)$$

This theory is the most basic description for a flexural wave traveling through a beam. A similar equation can be derived for plates. The theory will be limited to two dimensions

for ease of calculation.

A discussion of the assumptions is warranted. The effects of rotational inertia are ignored. This is valid as long as the wavelength of the flexural wave is much greater than the depth of the beam, thereby limiting the rotational velocity of beam elements. The second assumption is that plane sections remain plane. This is true only for beams in pure bending. Again this assumption is valid for waves with a wavelength comparable to or greater than the thickness of the beam (Kolsky, 1963). A more complete theory has been developed that does not make these assumptions (Timoshenko, 1921).

Next the conditions for the propagation of harmonic flexural waves are developed by assuming

$$y = De^{i(\gamma x - \omega t)} \quad (6.8)$$

where D is amplitude of the wave, ω is the radial frequency and γ is the wavenumber of the wave. The radial frequency and wavenumber can be described as

$$\omega = \gamma c_o \quad \gamma = \frac{2\pi}{\lambda} \quad (6.9)$$

where c_o is the phase velocity [meters/second] and λ is the wavelength [meters].

Although the wave propagating through the slab overlying a weak snowpack layer is not a harmonic wave, it is assumed that the flexural wave pulse travels at the same speed as a harmonic wave having the same wavelength (French, 1971). Substituting Equation 6.8 into Equation 6.7 yields an equation for the velocity of the propagating flexural wave.

$$c_o = \frac{2\pi}{\lambda} \sqrt{\frac{EI}{\rho A}} \quad (6.10)$$

The phase velocity, or wave velocity, is inversely proportional to the wavelength of the

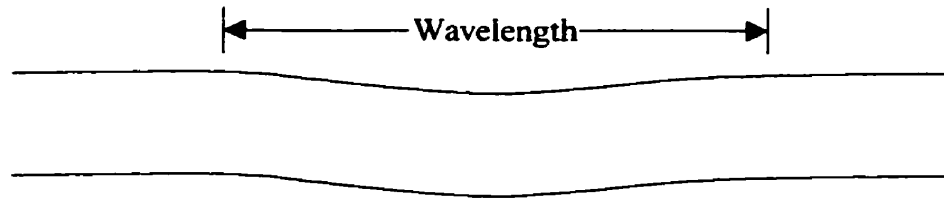


Figure 6.4 Bending of the overlying slab showing one wavelength.

propagating flexural wave.

The wavelength for the flexural wave that propagated in the snow slab on 19 February 2000 can be determined using Equation 6.9 and measurements at the site: a slab thickness of 0.39 m, a speed of 19.9 m/s, a density of the slab of 191 kg/m^3 which gives a Young's Modulus of 1 MPa (Shapiro et al., 1997). The calculated wavelength is 2.63 m (Figure 6.4). This wavelength is more than five times the thickness of the slab, which is consistent with the assumptions of ignoring rotational inertial effects and that plane sections remain plane.

6.5 Fracture of the Weak Layer as Result of the Bending Slab

In this section the forces generated in the slab due to a flexural wave are compared to those generated during the cantilever beam test. Figure 6.5 shows a bending slab created when the weak layer collapses. This diagram shows half of the bending slab in two dimensions. It is symmetrical about line QQ. The slab is rigidly attached to the weak layer in areas where the weak layer has not fractured. Figure 6.6 shows the free body diagram of the problem. Using classical mechanics of pure bending we can calculate the reaction forces exerted at the ends of the beam. The equation for the

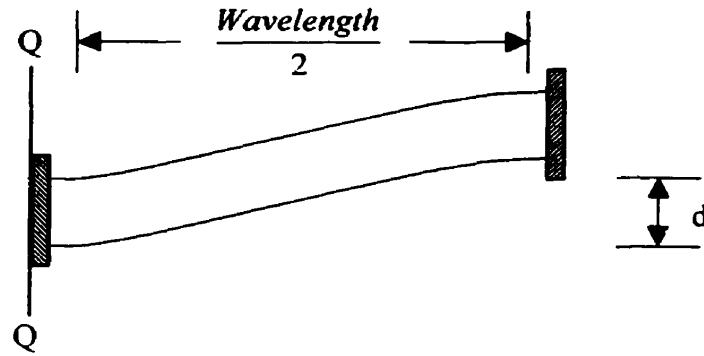


Figure 6.5 One half of the bending overlying slab. Its Assumed that the ends are fixed and that the length is one half of the wavelength in the slab.

moment at the end of each beam is

$$M = \frac{-6EId}{L^2} \quad (6.11)$$

where L is the length of the beam and d is the vertical displacement of one end of the beam relative to the other. Combining Equation 6.11 with Equation 6.10 yields the following equation

$$M = \frac{6c_o^2 h \rho d}{\pi^2} \quad (6.12)$$

where h is the thickness of the overlying slab. Using a downward displacement of 0.001 m the calculated moment at the end the bending slab is 18.0 N-m. This change in weak layer thickness corresponds to experimental data from 19 February 2000.

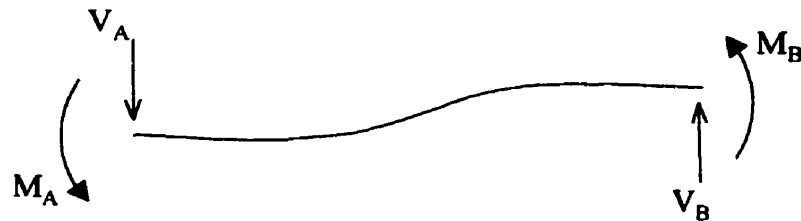


Figure 6.6 Free Body Diagram for a beam with both ends fixed. Forces in the x direction are negligible.

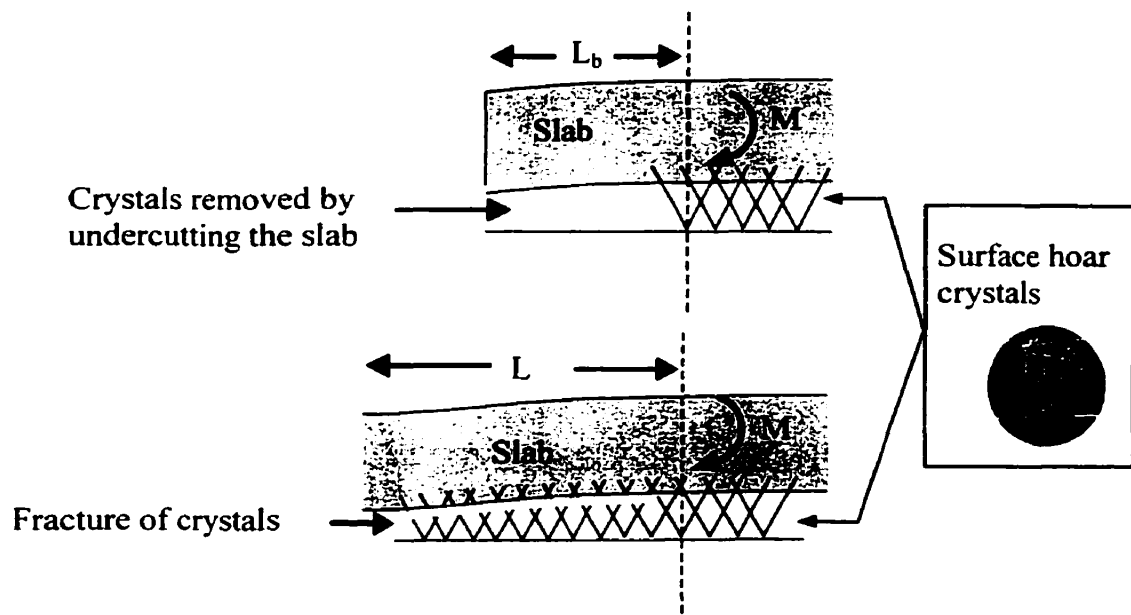


Figure 6.7 Schematic of the slab weak-layer interface for the cantilever beam (top) and a bending wave in the slab (bottom). The dashed indicates the area of maximum moment in the overlying slab. This corresponds to the area of largest shear stress and strain in the weak layer. Crystals of surface hoar are illustrated for the weak layer.

A discussion of the end conditions of the beam model is needed. It is assumed that the weak layer is rigidly connected to the overlying slab. Jamieson and Schweizer (2000) show that after a layer of surface hoar crystals is buried for an extended period, the surface hoar crystals have penetrated into the overlying slab (Figure 6.7). Longitudinal strains generated in the extreme fiber of the overlying slab are transferred as shear strain in the weak layer. While the exact shear stress distribution in the weak layer is unknown, it is assumed that the moment forces created by displacement of the overlying slab are similar to those created by cantilevering the overlying slab (Figure 6.7). The resulting shear stresses imposed on the weak layer would be similar. We can use the following equation to calculate the moment forces generated by the cantilever beam in the

overlying slab

$$M = \frac{1}{2} L_b^2 \rho h w g \quad (6.13)$$

Where L_b is the length of the cantilevered beam, ρ is mean density of the slab, g is acceleration due gravity and w is the width of beam. The calculated moment in the overlying slab for cantilever beam tests at failure on 19 February 2000 is 7.4 N-m. The average length of undercut (L_b) for these tests was 0.26 m.

It was already been shown in Chapter 5 that cantilevering the overlying slab can fracture the weak layer (Figure 5.8).

Calculations have shown that the moments generated by a flexural wave (18.0 N-m) in the overlying slab are similar to those

generated by adjacent cantilever beam tests (7.4 N-m). The resulting shear stresses and strains generated in the weak layer are also

expected to be quite similar. It is assumed that since any portion of the weak layer is loaded to fracture within 1s, the fractures are brittle (Narita, 1993). These simple calculations combined with experimental results from both fracture speed measurements and cantilever beam tests show that failure of the weak layer due to the bending of the overlying slab is a reasonable assumption.

While the weak layer is fractured in shear, the measured speed has shown that this is not a propagating fracture, but is instead a shear fracture of the weak layer that is coupled to a propagating flexural wave in the overlying slab.

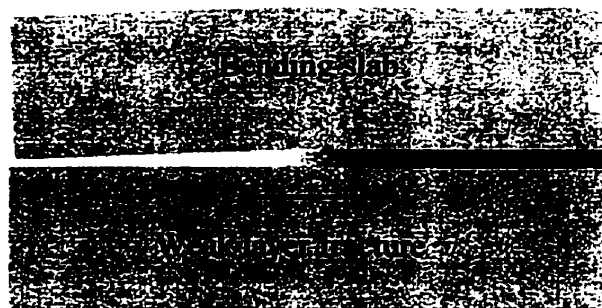


Figure 6.8 Bending of the overlying slab resulting in fracture of the weak layer.

6.6 Energy Considerations

In order for this coupled system to propagate the energy release rate must be greater than the fracture resistance. For a horizontal snow slab the energy supplied by the downward displacement of the slab must be greater than the fracture resistance in the weak layer for this fracture to propagate. The energy supplied by the downward displacement of the slab per unit area can be calculate using the following formula

$$Q = mgd \quad (6.15)$$

where m is the mass per unit area. Similarly, the energy (or the work of fracture per unit area) required to fracture the weak layer can be estimated using data from Föhn et al. (1998). They measured the force required to fracture the weak layer in shear, using a shear frame, and the shear displacement when fracture occurred. For surface hoar layers they found an average of 0.29 mm of displacement was required to fracture the weak layer. They also reported that the shear stress increased almost linearly with strain, indicating brittle failure. Using the measured strength value of 114.4 Pa for the surface hoar layer on February 19th and a displacement of 0.29 mm, the energy required to fracture surface hoar can be estimated at 0.03 J/m^2 . From Equation 6.15 the energy released from the downward displacement of the slab for 19 February 2000 can be calculated at 0.73 J/m^2 .

It is assumed that the fracture of the weak layer and the downward displacement of the overlying slab are coupled together and propagate at the same velocity radially outward from the trigger point. As this system propagates outward over a given distance the area of fractured weak layer approaches the area of overlying slab that displaces

downward (Figure 6.9). These assumptions allow the comparison of the energy released per unit area to the fracture resistance per unit area to determine if sufficient energy is present for fracture propagation. The energy per unit area released by the slab, 0.73 J/m^2 , is much greater than the energy required to fracture the weak layer, 0.03 J/m^2 . Sufficient energy is supplied by the overlying slab to fracture the weak layer in shear.

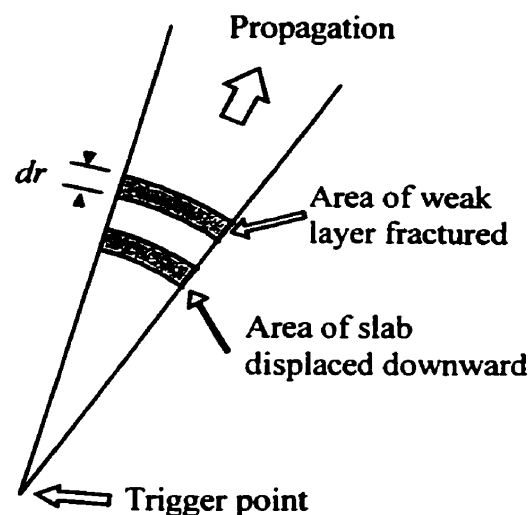


Figure 6.9 Plan view of fracture propagation in the weak layer coupled to the downward displacement of the overlying slab. The area for each is approximately equal for propagation over distance dr .

6.7 Source of Sound from a Whumpf

There are two obvious sources for sound generation when a whumpf occurs. The first source is the shear fracture of the weak layer. St. Lawrence and Bradley (1977) indicate that snow fracturing produces acoustic emissions that indicate changes taking place at the granular level within the snowpack. Certainly snow fracturing in shear will generate acoustic emissions. The question is whether sound generated in or near the weak layer could be transmitting through the snowpack at an audible level. Leird and Plehn (1984) report that snow has a very high attenuation rate, probably on the order of 500 db/m for a signal at 30 kHz . They indicate that to monitor the emission from a single crystal the sensor would have to be millimeters away from the crystal. Johnson (1978)

gives one of the most complete experimental and theoretical examinations of snow acoustics. He reports that the high loss of acoustic energy over 0.2 m to 0.4 m thick snowpack layers results in little sound transmission through a stratified snowpack. Johnson estimates transmission loss at 20 db to 80 db over snow layer with a thickness of 0.20 m to 0.40 m. This indicates that the sound generated when the weak layer is fractured could not be heard from an observer on the surface of the snow as a result of snow's high attenuation rates.

The second sound source could be sound generated by the flexural wave in the overlying slab. As previously stated flexural waves generate sound (Rossing and Fletcher, 1995). As bending of the overlying slab propagates outwards, sound is generated in the air by the displacement of the slab. Further experimental studies on the sound generated by whumpfs and remotely triggered avalanches would be worthwhile.

6.8 Discussion

There are several important field observations that help support this theory.

1. The first is that there is a measurable collapse of the weak layer at the site of whumpfs. The slab undoubtedly bends when this occurs, creating a flexural wave.
2. The velocity of fracture through weak layers on horizontal terrain has been estimated to travel as slow as 6 m/s and as fast as 300 m/s. This agrees with the fact that as flexural rigidity of a plate increases so too does the velocity of a flexural wave traveling through the plate.
3. An audible sound when a whumpf is triggered agrees with the fact that flexural waves produce much more sound than other any other type of elastic wave.

This failure theory includes several variables that are directly related to the snowpack variables measured in the field. Flexural stiffness (EI) of the overlying slab can be measured in the field and controls the wavelength and speed of a propagated flexural wave. This could explain why remotely triggered avalanches and whumpfs have stiffer and thicker overlying slabs (Table 4.4). Initially for younger, softer slabs flexural stiffness is very low, resulting in a longer flexural wavelength. The length is above the critical value to fracture the weak layer in shear. As the slab stiffens, over time and with additional snow, the wavelength decreases to below a critical value to fracture the weak layer in shear. This is when whumpfs and remotely triggered avalanches begin to occur.

This theory also offers an explanation for why whumpfs and remotely triggered avalanches tend to mainly occur on persistent weak layers, and why the weak layers for whumpfs and remotely triggered avalanches are thicker than for avalanches not remotely triggered. Downward displacement, when the weak layer fractures, is necessary to bend the overlying slab which then progressively fails the weak layer. This downward displacement releases gravitational potential energy, propagating the system. Persistent weak layers have a measurable thickness, and can collapse when they fracture. Other low density non-persistent weak layers might also collapse when fractured.

Looking at the entire system two conclusions can be drawn from this theory. The first is that the weak layer controls whether a whumpf or remotely triggered avalanche can occur, by collapsing when fractured. The second conclusion is that the

flexural stiffness of the overlying slab controls the window of time when a remotely triggered avalanche or whumpf can occur. Table 6.1 gives a qualitative overview of the fracture characteristics change with slab age. Most whumpfs and remotely triggered avalanches occur on medium age slabs. This is supported by the fact that shortest time between weak layer burial and a whumpf or remotely triggered avalanche is seven days with a median of 14 days for the 53 whumpfs and remotely triggered avalanches investigated.

| <i>Table 6.1 Weak layer fracture properties for different overlying slab ages.</i> | | | |
|--|--|---|--------------------------------------|
| | New snow slab (low stiffness) | Medium age slab (increasing stiffness) | Old slab (high stiffness) |
| Weak layer fracture | Common | Occasional | Rare |
| Propagation of fracture | Limited propagation ($< 2\text{m}$) | Favourable | Likely |
| Wavelength | Above critical value | Near critical value | Below critical value |
| Speed | NA | Slow | Fast |

7. CONCLUSIONS

- 1. Whumpfs and remotely triggered avalanches have different properties than avalanches that are not remotely triggered. The variables that showed significant differences were: weak layer age, weak layer thickness, weak layer crystal type, maximum crystal size of the weak layer, minimum crystal size of the weak layer, overlying slab thickness, overlying slab density, average hand hardness of the overlying slab and height of the snowpack.**
- 2. Collapse of the weak layer is essential for the propagation of fracture through a weak layer. This collapse provides the energy needed for fracture propagation.**
- 3. On low-angle terrain, fracture of a weak layer, triggered by an oversnow traveler, creates a bending wave in the overlying slab that progressively fractures the weak layer. The speed of this coupled system is governed by the flexural stiffness of the overlying slab.**
- 4. The properties of a weak snowpack layer govern whether a whumpf or remotely triggered avalanche will occur on that layer. The properties of the overlying slab govern the temporality of occurrence.**

5. A new technique for the cantilever beam test was developed that is repeatable and can be performed in the field. It can be used as an index for the flexural stiffness of a snow slab. When plotted against the density of the overlying slab, the results show less

scatter than previous studies.

While this thesis makes several conclusions about whumpfs and remotely triggered avalanches, one of the most important results of this research was the demonstration that macro scale experimental work on fracture propagation through weak snowpack layers is possible. Further experiments of this type are needed in order to understand avalanche release mechanisms better.

8. SUGGESTIONS FOR FUTURE RESEARCH

Future experimental research might include fracture propagation speed experiments, similar to the one presented here. Measurements on slabs with differing flexural stiffness might yield a correlation between speed of the propagating fracture and flexural stiffness. This would help to support the argument that a flexural wave travels in the overlying slab. Increasing the number of geophones, and possibly including multi-directional geophones would also be useful.

In addition to large scale experimental work, a smaller much more manageable project would be to record the sounds generated by whumpfs and remotely triggered avalanches. It is hypothesized that the frequency of this sound is determined by the wavelength and wave velocity of a flexural wave propagating through the overlying slab. Recording the sound of a whumpf would not require an elaborate experimental set-up and therefore could be repeated frequently.

One study that might prove worthwhile would be to monitor the temporal changes in the overlying slab, and relate these changes to the occurrence of whumpfs and remotely triggered avalanches. Cantilever beam tests performed on a slab overlying a weak layer as the slab ages might indicate when the slab has stiffened enough to propagate fractures through the weak layer.

REFERENCES

- Armstrong, B.R. and K. Williams. 1992. *The Avalanche Book*. Fulcrum Publishing. Golden, CO, 240 pp.
- Bader, H., R. Haefeli, E. Bucher, J. Neher, O. Eckel and C. Thams. 1954. *Snow and its Metamorphism*. Snow, Ice and Permafrost Research Establishment Translation 14. Cold Regions Research and Engineering Laboratory, Hanover, New Hampshire, 313 pp.
- Bader, H.P., and B. Salm. 1990. On the mechanics of snow slab release. *Cold Regions Science and Technology* 17: 287-300.
- Benson, C. 1960. PhD Thesis. California Institute of Technology.
- Bohren, C.F. and R.L. Beschta. 1974. Comment on "Wave Propagation in Snow." *American Journal of Physics* 42, 69-70.
- Bradley, C.C. and D. Bowles. 1967. Strength-load ratio, an index of deep slab avalanche conditions. *Physics of Snow and Ice*, (H. Oura, Ed.) Vol.1, Part 2, Institute of Low Temperature Science, Hokkaido University, Japan, 1243-1253.
- Bradley, C.C., R.L. Brown and T.R. Williams. 1977a. On depth hoar and the strength of snow. *Journal of Glaciology* 18(78), 145-147.
- Broek, D. 1986. *Elementary Engineering Fracture Mechanics*, fourth revised edition. Kluwer Academic, Hingham, MA, 516 pp.
- Bucher, E. 1948. Contribution to the theoretical foundations of avalanche defense construction. Snow, Ice and Permafrost Research Establishment, Translation 18, 1956, 99 pp.

- CAA. 1995. Observation Guidelines and Recording Standards for Weather, Snowpack and Avalanches. Canadian Avalanche Association. P.O. Box 2759, Revelstoke, BC, Canada, 98 pp.
- Colbeck, S, E. Akitaya, R. Armstrong, H. Gubler, J. Lafeuille, K. Lied, D. McClung and E. Morris. 1990. International Classification for Seasonal Snow on the Ground. International Commission for Snow and Ice (IAHS), World Data Center for Glaciology, U. of Colorado, Boulder, CO, USA.
- Daniels, H.E. 1945. The statistical theory of the strength of bundles of threads. Proceedings of the Royal Society of London, Series A, 183(995), 405-435.
- DenHartog, S.L. 1982. Firn quake. Cold Regions Science and Technology 6, 173-74.
- de Quervain, M. 1963. On the metamorphism of snow, In: Ice and Snow: Properties, Processes and Applications, M.I.T. Press, Cambridge, Mass., 377-390.
- Föhn, P.M.B. 1987. The Stability index and various triggering mechanism. International Association of Hydrological Science Publication 162. 195-211.
- Föhn, P.M.B., C. Camponovo and G. Krusi. 1998. Mechanical and structural properties of weak snow layers measured in situ. Annals of Glaciology 26. 1-6.
- Fredston, J. and D. Fesler. 1994. Snow Sense: A guide to evaluating snow avalanche hazard. Alaska Mountain Safety Center, Inc., Anchorage, Alaska, 116 pp.
- French, A.P. 1971. Vibrations and Waves. Norton Inc., New York, 316 pp.
- Fukuzawa, T. and H. Narita. 1993. An experimental study on the mechanical behavior of a depth hoar layer under shear stress. Proceedings of the International Snow Science Workshop in Breckenridge, Colorado, October 4-8. 1992. Colorado Avalanche Information Centre, Denver, Colorado, 80239 USA, 171-175.

- Geldsetzer, T. and B. Jamieson. 2000. Estimating dry snow density from grain form and hand hardness. In press for Proceedings of the International Snow Science Workshop in Big Sky Montana, October 2000.
- Georgi, J. 1933. Buried in the ice. Life at Mid-Ice Station during the last Greenland Expedition of Alfred Wegener. [Im Eis vergraben. Erlebnisse auf Station "Eismitte" der letzten Groenland-Expedition Alfred Wegeners] Muenchen, Mueller; 224 pp.
- Graff, K.F. 1955. Wave Motion in Elastic Solids. Ohio State University Press, Columbus, 649 pp.
- Gubler, H. and H.P. Bader. 1989. A model of initial failure in slab avalanche release. *Annals of Glaciology* 13, 90-95.
- Gubler, H. 1977. Artificial release of avalanches by explosives. *Journal of Glaciology*. 19(81). 419-429
- Haefeli, R. 1967. Some mechanical aspects on the formation of avalanches. *Physics of Snow and Ice*, (H. Oura, Ed.) Vol. 1, Part 2, Institute of Low Temperature Science, Hokkaido University, Japan, 1199-1213.
- Haefeli, R. 1963. Stress transformations, tensile strengths, and rupture processes of the snow cover, In: *Ice and Snow: Properties, Processes and Applications*, Edited by W. D. Kingery, M.I.T. Press, Cambridge, Massachusetts, 560-575.
- Hueter, T.F. and R.H. Bolt. 1955. *Sonics: Techniques for the use of Sound and Ultrasound in Engineering and Science*. Wiley Inc., New York, 456 pp.
- Jamieson, J.B. 1995. *Avalanche Prediction for Persistent Snow Slabs*. PhD Thesis, Dept. of Civil Engineering, University of Calgary, 275 pp.
- Jamieson, B. and T. Geldsetzer. 1996. *Avalanche Accidents in Canada, Vol. 4: 1984-96*. Canadian Avalanche Association, PO Box 2759, Revelstoke, BC, V0E 2S0, 202 pp.

- Jamieson, B. and T. Geldsetzer. 1999. Patterns in unexpected skier-triggered avalanches. *Avalanche Review* 18(3), 4-7.
- Jamieson, J.B. and C.D. Johnston. 1992a. Snowpack characteristics associated with avalanche accidents. *Canadian Geotechnical Journal* 29, 862-866.
- Jamieson, J.B. and C.D. Johnston. 1992b. A fracture-arrest model for unconfined dry slab avalanches. *Canadian Geotechnical Journal* 29, 61-66.
- Jamieson, J.B. and C.D. Johnston. 1998. Refinements to the stability index for skier-triggered slab avalanches. *Annals of Glaciology* 26, 296-302.
- Jamieson, J.B. and C.D. Johnston. Evaluation of the shear frame test for weak snowpack layers. Accepted for *Annals of Glaciology* 32.
- Jamieson, J.B. and J. Schweizer. 2000. Texture and strength changes of buried surface hoar layers with implications for dry snow-slab avalanche release. *Journal of Glaciology* 46(152), 151-160.
- Johnson, J.B. 1978. *Stress Waves in Snow*. PhD Dissertation, University of Washington, Seattle, WA, 148 pp.
- Johnson, B.C., J.B. Jamieson and C.D. Johnston. 2000. Field data and theory for human triggered "whumpfs" and remote avalanches. *Proceedings of the International Snow Science Workshop at Big Sky, MT, October 1-8, 2000*.
- Kirchner, H.O.K., G. Michot and T. Suzuki. 2000. Fracture toughness of snow in tension. *Philosophical Magazine* 80, No.5, 1256-1272.
- Kolsky, H and Rader. 1963. *Stress Waves in Solids*. Dover Publications, Inc., New York, NY, 213 pp.

- Lackinger, B. 1989. Supporting forces and stability of snowslab avalanches: a parameter study. *Annals of Glaciology* 13, 140-145.
- Leaird, J.D. and J. Plehn. 1984. Acoustic emission monitoring on avalanche prone slopes. *Third Conference on Acoustic Emission/Microseismic Activity in Geologic Structures and Materials*. The Pennsylvania State University, October 5-7, 449-460.
- Leprettre, B., J.P. Navarre, A. Taillefer, Y. Danielou, J.M. Panel and F. Touvier. 1996. Reliable estimation of avalanche activity using seismic methods. *Proceedings of the International Snow Science Workshop in Banff, Alberta, October 6-11, 1996*, 184-189.
- Mann, H.B. and D.R. Whitney. 1947. On a test of whether one of two random variables is stochastically larger than the other. *Ann. Math. Statist.* 18. 50-60.
- McClung, D.M. 1979. Shear fracture precipitated by strain softening as a mechanism of dry slab avalanche release. *Journal of Geophysical Research* 84(B7), 3519-3526.
- McClung, D.M. 1981. Fracture mechanical models of dry slab avalanche release. *Journal of Geophysical Research* 86(B11), 10783-10790.
- McClung, D.M. 1987. Mechanics of snow slab failure from a geotechnical perspective, *In: B. Salm and H. Gubler, eds., Avalanche Formation, Movement and Effects*. International Association of Hydrological Sciences, Publication No. 162, New York, 475-507.
- McClung, D.M. and P.A. Schaerer. 1993. *The Avalanche Handbook*. The Mountaineers, Seattle, 271 pp.
- Mears, A. I. 1998. Tensile strength changes in new snow layers. *Proceedings of the International Snow Science Workshop in Sunriver, OR, September 27- October 1, 1998*, 574-576.

- Narita, H. 1983. An experimental study on the tensile fracture of snow. Contributions from the Institute of Low Temperature Science, Contribution No. 2625, Institute of Low Temperature Science, Hokkaido University, Sapporo, Japan, 1-37.
- Neave, H.R. and P.L. Worthington. 1988. Distribution-Free Tests. Unwin Hyman, London, 430 pp.
- Palmer, A.C. and J.R. Rice. 1973. The growth of slip surfaces in the progressive failure of overconsolidated Clay, Proceedings of the Royal Society, Vol. A 332, 527-548.
- Perla, R.I. 1969. Strength tests on newly fallen snow. Journal of Glaciology 8, No. 54, 427-440.
- Perla, R.I. 1977. Slab avalanche measurements. Canadian Geotechnical Journal 14(2), 206-213.
- Perla, R.I. 1980. Avalanche release, motion and impact, In: Dynamics of Snow and Ice Masses, Edited by S.C. Colbeck, Academic Press, New York, 397-462.
- Perla, R.I. and E.R. LaChapelle. 1970. A theory of snow slab failure. Journal of Geophysical Research 75(36), 7619-7627.
- Roch, A., 1956. Mechanism of avalanche release, U.S. Army, Snow, Ice and Permafrost Research Establishment, Hanover, New Hampshire, Translation 52, 11 pp.
- Rossing, T.D. and N.H. Fletcher. 1995. Principles of Vibration and Sound. Springer-Verlag New York Inc, New York, NY, 282 pp.
- Scott, C. 1994. Summits and Icefields. Rocky Mountain Books, Calgary, Alberta, 304 pp.
- Schaerer, P.A. and A.A. Salaway. 1980. Seismic and impact-pressure monitoring of flowing avalanches. Journal of Glaciology 26(94), 179-187.

- Schwarz, J., Frederking, R., Gavrillo, V., Petrov, I.G., Hirayama, K.I., Mellor, M., Tryde, P. and K.D. Vaudry. 1981. Standardized testing methods for measuring mechanical properties of ice. *Cold Regions Science and Technology* 4, 245-253.
- Schweizer, J. 1999. Review on the role of deficit zones on dry snow slab avalanche release. *Cold Regions Science and Technology* 30(1-3), 43-57.
- Seligman, G. 1936. *Snow Structure and Ski Fields*. International Glaciological Society, Cambridge, 555 pp.
- Shapiro, L.H., J.B. Johnson, M. Sturm, and G.L. Blaisdell. 1997. *Snow mechanics: review of the state of knowledge and application*. US Army CRREL Report 97-3.
- Shapiro, S.S, M.B. Wilk and H.J. Chen. 1968. A comparative study of various tests for normality. *American Statistical Association Journal*, 1343-1372.
- Sommerfeld, R.A. 1969. The role of stress concentration in slab avalanche release. *Journal of Glaciology* 8(54), 451-462.
- Sommerfeld, R.A. 1977. Preliminary observations of acoustic emissions preceding avalanches. *Journal of Glaciology*, 19(81), 399-409
- Sommerfeld, R.A. 1980. Statistical models of snow strength. *Journal of Glaciology* 26(94), 217-223.
- Sommerfeld, R.A. 1982. A review of snow acoustics. *Reviews of Geophysics and Space Physics* 20(1), 62-66.
- Sommerfeld, R.A. and H. Gubler. 1983. Snow avalanches and acoustic emissions. *Annals of Glaciology* 4, 271-276.
- St. Lawrence, W., and C. Bradley. 1977. Spontaneous fracture initiation in mountain snow-packs. *Journal of Glaciology* 19(81), 411-417.

- Sterbenz, C. 1998. The cantilever beam or "Bridgeblock" snow strength test. Proceedings of the International Snow Science Workshop in Sunriver, OR, September 27-October 1, 1998, 566-573.
- Sterns, R.C. 1964. Flexural properties of snow and snow-ice. Cold Regions Research and Engineering Laboratory Special Report 59.
- Stethem, C.J. and J.W. Tweedy. 1981. Field tests of snow stability, In: Proceedings of the Avalanche Workshop in Vancouver, November 3-5, 1980, Edited by Canadian Avalanche Committee, National Research Council of Canada, Technical Memorandum No. 133, 52-60.
- Timoshenko, S.P. 1921. On the correction for shear of the differential equation for transverse vibration of prismatic bars. *Philosophical Magazine* 43, No. 6, 125-131.
- Truman, J.C. 1973. Wave propagation in snow. *American Journal of Physics* 41, 282-283.
- Wilson, J.T. 1955. Coupling between moving loads and flexural waves in floating ice sheets. Snow, Ice and Permafrost Research Experiment report 34.

APPENDIX A

Data collected from whumpfs and remotely triggered avalanches are compared to data collected from avalanches that were not remotely triggered using the Kolmogorov-Smirnov test. This test is used for fourteen snowpack variables to look for a difference in location (mean). This test uses the maximum vertical difference between the cumulative distribution functions as the test statistic (Neave and Worthington, 1988 p. 152). The comparisons for the fourteen variables are presented in Table A.1: weak layer age, weak layer thickness, maximum crystal size of the weak layer, minimum crystal size of the weak layer, shear strength of weak layer, weak layer temperature, slab thickness, slab density, load on weak layer, average slab hardness, compression test score, stability index, rutchblock score and height of snowpack. The results obtained using this test showed significant differences for the same variables as were found in Chapter 4.

Table A.1 Kolmogorov-Smirnov test for differences.

| Variable | | Whumpfs and remotely triggered avalanches | Avalanches not remotely triggered | <i>p</i> |
|-----------------------|--|---|-----------------------------------|-------------------|
| | | Mean | Mean | |
| Weak layer properties | Weak layer age (days) | 19.4 | 10.9 | < 0.005 |
| | Weak layer thickness (mm) | 3.6 | 1.2 | < 0.001 |
| | Maximum crystal size (mm) | 10.1 | 4.0 | < 0.001 |
| | Minimum crystal size (mm) | 5.3 | 2.7 | < 0.005 |
| | Shear strength (kPa) | 0.76 | 0.62 | > 0.10 |
| | Weak layer temperature (°C) | -3.9 | -4.4 | > 0.10 |
| Slab properties | Slab thickness (cm) | 63.2 | 43.1 | < 0.005 |
| | Slab density (kg/m³) | 148.2 | 127.4 | < 0.005 |
| | Load on weak layer (kPa) | 98.4 | 64.2 | < 0.025 |
| | Average slab hardness | 1 Finger | 4 Finger | < 0.001 |
| Stability indices | Compression test score | 15.8 | 15.4 | > 0.10 |
| | Stability index | 0.80 | 0.77 | > 0.10 |
| | Rutchblock score | 4.1 | 3.8 | > 0.10 |
| | Height of snowpack (cm) | 179 | 315 | < 0.001 |

¹ Rows for which $p \leq 0.05$ are marked in bold.